MODELING AND ANALYSIS OF HIGHWAY EMISSIONS DISPERSION DUE TO NOISE BARRIER SHAPE EFFECTS AND TRAFFIC FLOW UNDER DIFFERENT INFLOW CONDITIONS

by

Shaoguang Wang

A Thesis

Submitted to the Faculty of Purdue University

In Partial Fulfillment of the Requirements for the degree of

Master of Science in Mechanical Engineering

Department of Mechanical and Civil Engineering

Hammond, Indiana

May 2020

THE PURDUE UNIVERSITY GRADUATE SCHOOL
STATEMENT OF COMMITTEE APPROVAL

Dr. Xiuling Wang, Chair

Department of Mechanical and Civil Engineering

Dr. Nesrin Ozalp

Department of Mechanical and Civil Engineering

Dr. Ran Zhou

Department of Mechanical and Civil Engineering

Dr. Wubeshet Woldemariam

Department of Mechanical and Civil Engineering

Approved by:

Dr. Chenn Zhou

ACKNOWLEDGMENTS

My sincere gratitude goes first to my advisor, Dr. Xiuling Wang, for her constant encouragement and guidance. She had been providing me with a lot of precious research skills and valuable advice for my thesis. She is always patient to help me overcome obstacles and challenges in my study. Her strong passion in the academic field is the goal I will pursuit for the rest of my research and career.

Secondly, I would like to thank all staff and faculty in the department of Mechanical and Civil Engineering in Purdue Northwest. They are always prepared to answer various questions and working as a competitive team. All courses I took in the past years help me a lot when I did this research. I am grateful for Dr. Nesrin Ozalp, Dr. Ran Zhou and Dr. Wubeshet Woldemariam who are willing to be the members of examining committee.

Finally, my thanks would go to my beloved family and friends who stand by me with their understanding, support and love.

TABLE OF CONTENTS

LIST OF TABLES

LIST OF FIGURES

NOMENCLATURE

ε	turbulence dissipation rate
ρ	density
μ	viscosity
σ_k	turbulence Prandtl number for k, 1.0
σ_ε	turbulence Prandtl number for ε, 1.2
C^*	normalized concentration
$C_{1\varepsilon}$	constant 1.44
C_2	constant 1.9
G_b	generation of turbulence kinetic energy due to buoyancy
G_k	generation of turbulence kinetic energy due to the mean velocity gradients
H	noise barrier height
h	vehicle height
I	turbulence intensity
$\vec{J_i}$	diffusion flux of species i
k	turbulence kinetic energy
L_x	length of emission source
L_y	width of emission source
$\bar{p}$	time averaged pressure
Q	volumetric flow rate
R_i	net rate of production of species i by chemical reaction
S_i	rate of creation by any addition
$\bar{S}_{ij}$	rate-of-strain tensor for the resolved scale
S_k	user-define source term
S_ε	user-define source term
t	time
$\bar{U}_i$	time averaged mean velocity in x-direction
$\bar{U}_j$	time averaged mean velocity in y-direction
$U(z)$	velocity at height z

$U(z_r)$	reference velocity
x_i	x-direction
x_j	y-direction
Y_i	local mass fraction of species i
Y_k	dissipation of k due to turbulence
Y_M	contribution of the fluctuating dilatation in compressible turbulence to the overall dissipation rate
$\vec{v}$	velocity
z	height
z_r	reference height

ABSTRACT

A three-dimensional computational fluid dynamics (CFD) model has been developed to simulate the distribution of automobile emissions on and near a highway. A variety of k-ε turbulence models were adopted to simulate the turbulence flow, and a non-reaction species model was coupled to simulate the dispersion of emissions. The models were first validated by comparing velocity profiles and normalized emission concentration with wind tunnel experiments, and good agreement was observed. Next, further simulation and analysis revealed that T-shaped noise barriers could reduce more emissions concentration in downstream areas than rectangular noise barriers; however, the noise barrier shape effects on the dispersion of emissions were also influenced by inflow conditions. Thirdly, the traffic flow conditions on the highway made a difference to the dispersion of emissions. Automobile wakes not only existed behind vehicles but also induced turbulence on adjacent lanes, causing more emissions on the highway. Low traffic speed, such as congestion, would result in more emissions remaining on the highway as well. At last, vehicle body shapes modified the flow patterns by their slant angles and heights. Vehicles with slant angles on both front and rear sides had the least concentration of emissions at the center of the highway.

1. INTRODUCTION

1.1 Background and Motivation

Automobile emissions, being one of the major causes of air pollution, is a serious global problem. In addition to its negative influence on the environment, the toxic gas and granules in the automobile emissions, including nitrogen oxides (NOx), carbon monoxide (CO) and particle matter (PM), can cause some symptoms and diseases among people, especially young children, who live in the proximity of heavily trafficked highways [1]. Figure 1 is a Google Maps search result of schools in Lake County, Indiana, in which many schools are located near highways. Previous health report revealed that automobile emissions could cause prematurity and low birth weight among mothers [2] and respiratory diseases to residents [3]. As a result, it is important to study the dispersion of automobile emissions near highways as considering the environment and the health care.

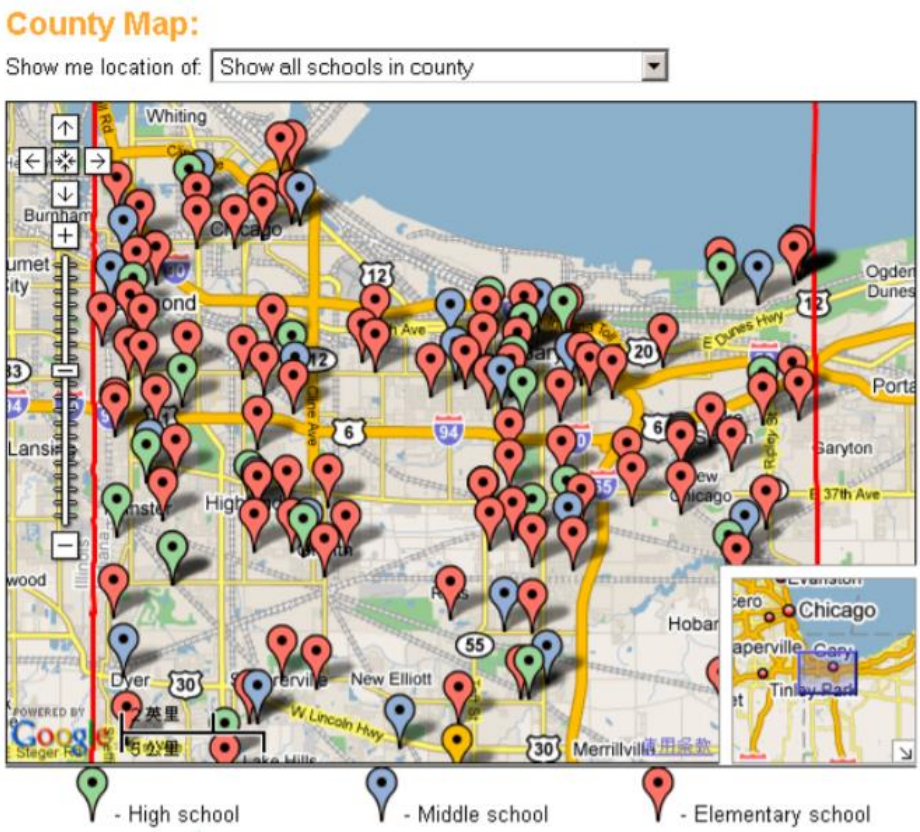

Figure 1. Locations of schools near major highways in Lake County, IN

According to the Environmental Protection Agency (EPA), vehicles that are larger, heavier, and more powerful generally, have lower fuel economy and higher CO2 emissions than other comparable vehicles. The mix of vehicles in the type of sedans or wagons have an average weight that is still 13% below 1975 values, but trucks are now almost 30% heavier than in model year 1975. Vehicle power and acceleration have increased across all vehicle types [4]. Highway noise barriers were originally designed to protect communities near highways from vehicle noise. Recent study has suggested that roadside barriers have positive effects on reducing downstream emission concentration. The level of reduction can be determined by a variety of factors, such as roadway configuration, local meteorology, barrier height and other factors [5]. Further detailed studies and simulation will be necessary for understanding some effects of dominated factors. It will provide valuable suggestions on guidelines for noise barriers design and on traffic flows traveling on highways.

1.2 Literature Review

The effects of noise barrier on the dispersion of automobile emissions have been studied in various manners. Some of the well-known methods are wind tunnel experiments, data collection directly from field research, and computational simulation and analysis.

A commonly cited study is the wind tunnel study published by Heist et al., 2009 [6]. They modeled 12 different roadway configurations, including noise barriers and roadway elevation or depression, and discussed the effect of those configurations on the dispersion of traffic emission. The study concluded that all 12 configurations reduced the downstream near-ground concentration compared with that for a flat and unobstructed roadway [6]. Amini et al., 2016, found that a 4 m high barrier resulted in a 35% reduction in average concentration within 40 m of the barrier, relative to the no-barrier site. Also, the concentration reduction could be 55% if the barrier height was doubled [7]. Previous research also focused on noise barrier side edge effects under different thermal conditions, but only rectangular noise barriers were studied [8].

Because noise barriers are designed to suppress the spread of noise, the way noise barriers affect emissions dispersion is different than the way they impede sound propagation, so governing equations and mechanisms are completely different. A lot of research has focused on the acoustic

performance of barriers with different shapes and surface conditions [9–13]. Scholes et al. carried out field research to obtain the acoustic performance of full-scale noise barriers of various heights under a range of wind conditions [9]. Ishizuka and Fujiwara introduced a different type of commonly used noise barrier in their paper [10], as shown in Figure 2. They tested the acoustic performance of common noise barriers using the boundary element method (BEM) and suggested that the soft T-shaped barrier had the best results in noise reduction. Baulac et al. analyzed the acoustical efficiency of T-shaped noise barriers whose top is covered with a series of wells [11]. Unfortunately, the study of barrier shape effect was limited on acoustic performance. To the best of the authors' knowledge, there was no further study about the noise barrier shape effect on highway emission dispersion in the literature.

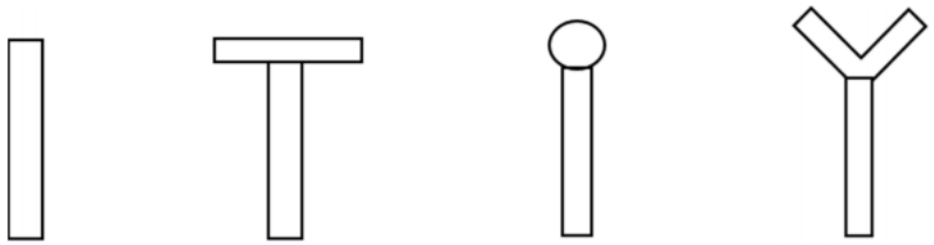

(a) Rectangular (b) T-shaped (c) Cylindrical (d) Y-shaped (branched)

Figure 2. Different shapes of commonly used noise barrier

Besides field study and wind tunnel testing, numerical simulation has become prevalent due to the rapid development of computational resources and techniques. A numerical study by Hagler et al., 2011 matched the previous wind tunnel study. Their results further implied that roadside barriers may mitigate near-road air pollution [14]. Furthermore, Finn et al. conducted a roadway toxics dispersion study to document the effects on concentrations of roadway emissions behind a roadside sound barrier in various conditions of atmospheric stability [15]; and Steffens et al. modeled a solid noise barrier under various atmospheric stability conditions by employing Reynolds Averaged Navier-Stokes (RANS) and Large Eddy Simulation (LES) models [16].

As mentioned above, the level of pollutant reduction can be determined by the local meteorology and inflow conditions. Three inflow conditions were adopted in this study: (1) uniform inlet wind profile without wind shear, which is commonly used in wind tunnel testing; (2) linear wind shear profile, which has the same mass flow rate as the uniform inlet wind profile; (3) normal wind

profile, steady vertical wind shear, which uses a power law velocity profile [17]. The existence of wind shear could create a very complex wake structure with substantial asymmetries, streamwise vorticity generation, and non-periodicities [18]. Consequently, the wake and turbulence were expected to influence the downstream dispersion of emissions.

Speaking of wake and turbulence, recent research has found that the automobile wake flow also induces strong effects on emissions dispersion. First, Rao et al. proposed that traffic-induced turbulence plays a dominant role in the dispersion of pollutants near highways because the wakes behind moving vehicles contain organized trailing vortices which rapidly mix the pollutants released in the turbulent wake, and they discussed the formulations for velocity deficit and turbulence in vehicle wakes from theoretical and physical modelling studies [19]. Alonso-Estebanez et al. focused on traffic-induced turbulence analysis from a field experimental study. They attempted to build the relationship between vehicle speed and turbulent kinetic energy (TKE) for different types of vehicles [20]. Bhautmage et al. studied effects of moving-vehicle wakes on pollutant dispersion inside a tunnel, and their results showed that wakes accelerated the piston effect and varied with the size, shape and speed of vehicles [21]. Carpentieri et al. conducted wind tunnel measurements for modelling the regions of vehicle wakes: near-wake and far-wake [22]. Karim et al. developed a mathematical model to identify street canyon and vehicle wake effects on the transport air pollution from urban road microenvironments [23]. Dong et al. simulated traffic congestion and traffic flow in urban roadway tunnels, and their results revealed that near-ground region and tunnel downstream were high pollutant concentration regions [24]. Huang et al. studied the vehicle queue effect on exhaust dispersion in the vehicle wake through a wind tunnel experiment and showed that the flow behind vehicles can provide different shapes of exhaust scalar dispersion fields in the vehicle wake [25]. Kim et al. quantified vehicle induced turbulence (VIT) for complex traffic scenarios by CFD simulation and implied that there was not a big difference in the volume-averaged TKE values when vehicles were moving in the same or the opposite direction [26]. Therefore, two-way traffic can be treated as one-way traffic.

Evidently, numerous researches have focused on the wake flow and on automobile emissions for the purpose of the environment. There are a variety of field research, wind tunnel experiments, and computational simulation that are applied to investigate highway configurations and the wake

flow. However, few researches have ever combined comprehensive effects to analyze the interaction. The work presented in this paper first studied effects of highway configurations, i.e. noise barriers, and inflow conditions. Then the automobile wake flow and its interaction were combined with highway configurations. As a consequence, the effects on emissions dispersion can be simulated much closer to the reality.

2. METHODS AND METHODOLOGY

2.1 Wind Tunnel Experiments Review

2.1.1 Noise Barriers in Wind Tunnel

In order to make sure simulation results reasonable, the computational model for noise barrier shape effects and influence of inflow conditions in this paper was first validated with a wind tunnel experiment conducted by Heist et al. [6]. The wind tunnel was a 1:150 model (18.3 m × 3.7 m × 2.1 m), and the tracer gas, ethane (C_2H_6), represented the automobile emission on the highway. The rectangular noise barrier was 6 m high (H) in the full scale and spanned along the highway. The computational domain in this paper was consistent with the wind tunnel experiment and had the same dimensions as the wind tunnel configuration. The x-axis was extended along with the wind direction perpendicular to the highway. The highway was 2 m away from the inlet and treated as the emission source. The highway noise barrier was 0.04 m high, 0.003 m thick (6 m high, 0.5 m thick in the full scale). The computational domain is shown in Figure 3.

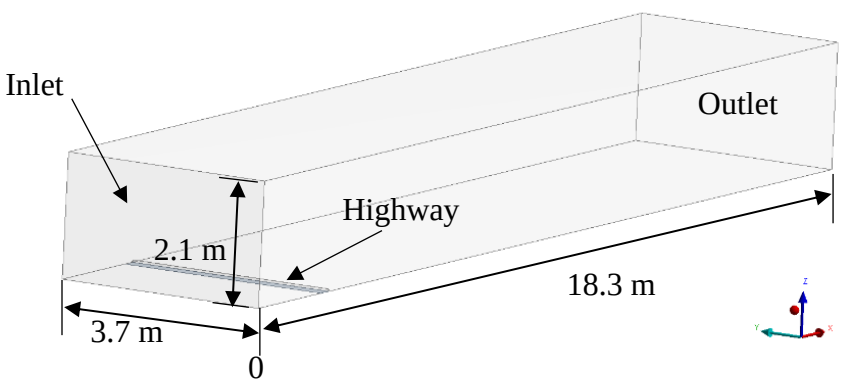

(a) Overall view

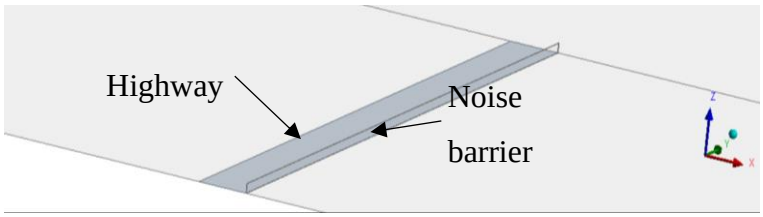

(b) Close view of highway and noise barrier

Figure 3. Computational domain for noise barriers

2.1.2 Traffic Flow in Wind Tunnel

The second computational domain used for validation of traffic flow was compared with another wind tunnel experiment, which was done by Carpentieri et al. [22]. Their wind tunnel was 20-meter-long, 3.5-meter-wide and 1.5-meter-high. A 1:5 scaled model was placed in it to represent the moving vehicle. The scaled car was 860-mm-long, 380-mm-wide and 300-mm-high. The flow condition had a reference wind speed 2.5 m/s at a reference height 1 m. The wind attacked right at the front face of the car model. A tailpipe was attached behind the vehicle model in the wind tunnel experiment to discharge the tracer gas, propane (C_3H_8), at a constant flow rate of 0.33 m/s. Then velocity profiles and normalized concentration of the tracer gas were measured at two locations behind the vehicle.

In wind tunnel measurements, a common practice is to place the car model near the edge of a raised false floor in order to get rid of the effects of the bottom wall. Accordingly, the car model in the computational domain was lifted up to 240 mm from the ground and offset by 11 m from the inlet to the domain. The coordinate system for the computational domain was defined as follows: x-direction was the wind flow direction with x = 0 at the rear of the car; y-direction was the span of the computational domain with y = 0 at the symmetry axis; z-direction was the vertical height with z = 0 at the ground level. The computational domain is shown in Figure 4.

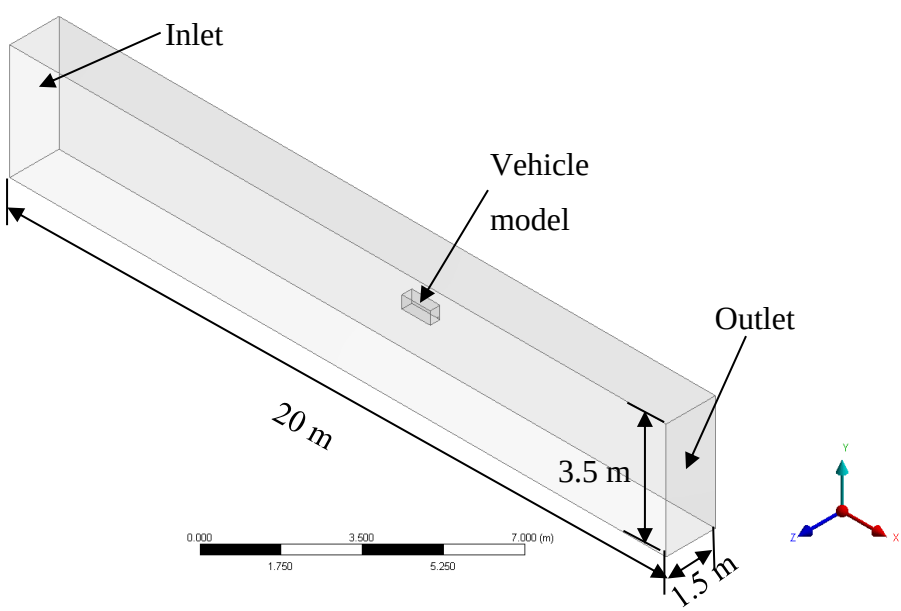

Figure 4. Computational domain for traffic flow

2.2 Wind Inflow Conditions

Three inflow conditions were studied in this paper. The first one was the uniform inflow condition, which introduced a constant wind speed at 7 m/s [17]. The second one was the linear approximation to the power law, which was expressed as [17]

$$u(z) = 5.1\left(\frac{z}{24.4} + 0.5\right) + 4.45, \tag{1}$$

When height was zero, the wind speed reached the same speed as the uniform inflow condition. The last one, which was also a commonly used one, was the power law. Its governing equation was described as [17]

$$u(z) = 7\left(\frac{z}{10}\right)^{0.35}, \tag{2}$$

The reference height in the power law was 10 m, so the reference velocity would be consistent with the uniform inflow condition, 7 m/s. The wind profile determined by three inflow conditions is shown in Figure 5. To better display the linear approximation to the power law, the height in Figure 5 was offset to the height of a wind turbine, 12.2 m [17].

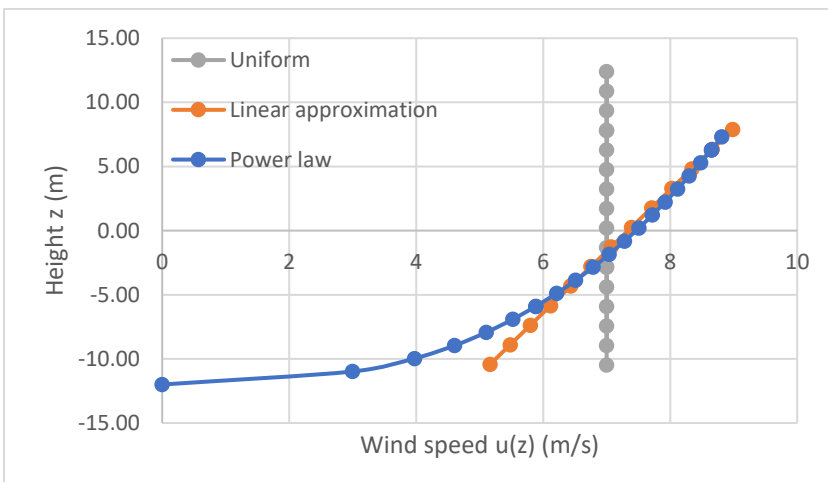

Figure 5. Wind inflow conditions

2.3 Turbulence Models

Commercial software ANSYS® Fluent 19.1 was used in the numerical simulation. ANSYS Fluent contains the broad, physical modeling capabilities needed to model flow, turbulence, heat transfer and reactions for industrial applications. RANS averages parameters in Navier-Stokes equations on time and simulates all the turbulence scales; LES averages the parameters on space so that large

eddies could satisfy governing equations and simulate only the smallest eddies. Reynolds Averaged Navier-Stokes (RANS) modeling is a widely used scheme for simulating turbulent flow because it is relatively accurate and computationally efficient compared to Large Eddy Simulation (LES). Therefore, RANS model was adopted in this paper considering timesaving. RANS equation was expressed as [27]

$$\rho\left(\frac{\partial \bar{U}_i}{\partial t}+\bar{U}_j\frac{\partial \bar{U}_i}{\partial x_j}\right)=\frac{\partial}{\partial x_j}\left(\mu\frac{\partial \bar{U}_i}{\partial x_j}-\rho\overline{U_i U_j}\right)-\frac{\partial \bar{p}}{\partial x_i}, \tag{3}$$

Different turbulence models, including standard/RNG/realizable k-ε model and standard/SST k-ω model were tested in this study. The major differences in three k-ε models are the method of calculating turbulent viscosity, the turbulent Prandtl numbers governing the turbulent diffusion of k and ε, and the generation and destruction terms in the ε equation [28]. The major differences in two k-ω models are the gradual change from the standard k-ω model in the inner region of the boundary layer to a high-Reynolds number version of the k-ε model in the outer part of the boundary layer and the modified turbulent viscosity formulation to account for the transport effects of the principal turbulent shear stress [29]. The simulation results were compared at the beginning in order to find a better model that can give valid results. Finally, the realizable k-ε model was selected due to its best match with the wind tunnel experimental data. The governing equations for the turbulence kinetic energy, k, and the turbulence dissipation rate, ε, in the realizable k-ε model are described as [30]

$$\frac{\partial}{\partial t}(\rho k)+\frac{\partial}{\partial x_j}(\rho k u_j)=\frac{\partial}{\partial x_j}\left[\left(\mu+\frac{\mu_t}{\sigma_k}\right)\frac{\partial k}{\partial x_j}\right]+G_k+G_b-\rho\varepsilon-Y_M+S_k, \tag{4}$$

and

$$\frac{\partial}{\partial t}(\rho\varepsilon)+\frac{\partial}{\partial x_j}(\rho\varepsilon u_j)=\frac{\partial}{\partial x_j}\left[\left(\mu+\frac{\mu_t}{\sigma_\varepsilon}\right)\frac{\partial \varepsilon}{\partial x_j}\right]+\rho C_1 S\varepsilon-\rho C_2\frac{\varepsilon^2}{k+\sqrt{\nu\varepsilon}}+C_{1\varepsilon}\frac{\varepsilon}{k}C_{3\varepsilon}G_b+S_\varepsilon, \tag{5}$$

where

$$C_1=max\left[0.43,\frac{\eta}{\eta+5}\right],\eta=S\frac{k}{\varepsilon},S=\sqrt{2S_{ij}S_{ij}}, \tag{6}$$

2.4 Species Transport Model

As this paper focused more on the distribution of species instead of the chemical reactions between them, the non-reaction species transport model was selected to simulate the transportation and

dispersion of the automobile emissions. The general form in the non-reaction species transport equation for the *i*th species is expressed as [31]

$$\frac{\partial}{\partial t}(\rho Y_i) + \nabla \cdot (\rho \vec{v} Y_i) = -\nabla \cdot \vec{J_i} + R_i + S_i, \tag{7}$$

where R_i was 0 in this study due to no chemical reactions occurring in the computational domain.

Carbon monoxide (CO) was used as the tracer gas to represent the emissions in the later simulation in this paper. However, the tracer gas was ethane when validating the species model in order to be consistent with the wind tunnel experiment, and its concentration was normalized to a dimensionless concentration, given by [6]

$$C^* = \frac{Y L_x L_y U(z_r)}{Q}, \tag{8}$$

where L_x, L_y were width and length of the emission source, which were 0.24 m and 3.7 m, respectively; $U(z_r)$ was the reference velocity 2.46 m; Q was the volumetric flow rate of the emission, 1500 cc/min; Y is mass fraction recorded in the domain.

2.5 Traffic Flow

In addition to noise barriers beside the highway, one-way traffic flow was added on the highway. Only one-way traffic was simulated in this paper because there was not a big difference of the turbulent kinetic energy in traffic flows when vehicles moved in the same or the opposite direction [26]. In this scenario, the computational domain was not a scaled model as the ones used before. The three-dimensional computational domain was 100-m-long, 40-m-wide, and 30-m-high. In the domain, one-way six-lane highway was generated first. Each lane had a width of 3 meters and spanned the full length of the computational domain. Only the centerlines of the traffic lane were present in Figure 6 because the centerlines were used as the symmetry axis of the vehicles. As shown in Figure 6, a highway computational domain in the shadowed area was created on the highway to define local fine mesh as intensive turbulence was supposed to be formed on the highway area due to the fast-moving traffic flow.

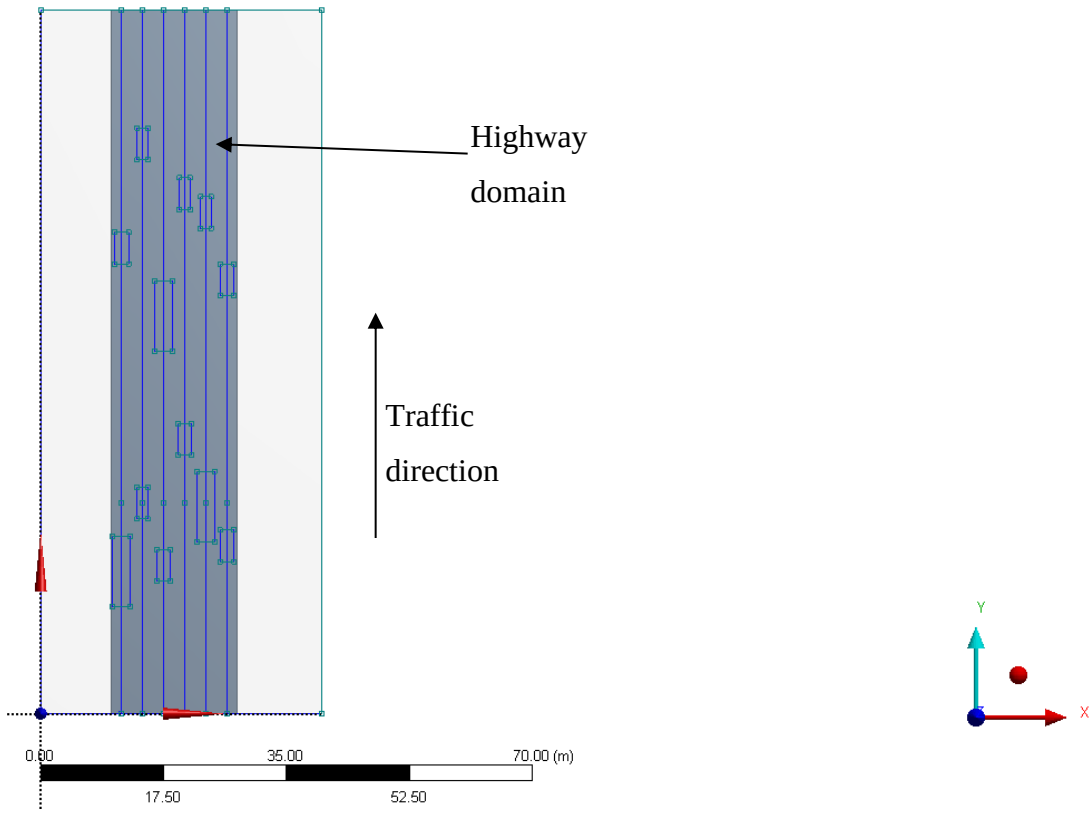

Figure 6. Computational domain of traffic flow on highway

The geometry of vehicles in the domain is shown in Figure 7. All vehicles moved along the positive direction of y-axis. There were three types of vehicles on the highway: sedan, SUV, and truck. The dimensions of the vehicle bodies were 4.5 m × 1.5 m × 1.5 m for sedan, 4.5 m × 2 m × 2 m for SUV, and 10 m × 2.5 m × 3 m for truck, whereas sedan and SUV had a 30º slant angle at the front, and sedan had another 45º slant angle at the rear [21]. All vehicles were placed on the highway randomly, but the distance between two vehicles in the same lane followed the safe driving operation: the following car stays at least two to three seconds behind the vehicle ahead [33]. Even though none of tires were included when building vehicle models, ground clearance was set 0.2 m for sedan and 0.3 m for SUV and truck respectively. A circle was attached on the rear face of each vehicle to represent vehicle's exhausting pipe, and they were defined as emissions sources in the simulation. The diameter was 0.04 m for sedan and SUV, and 0.06 m for truck. Considering that exhausting pipes are mounted either on the left or on the right or that some vehicles even have double exhausting pipes, the exhausting pipe was created on the middle of vehicles for simplification in this paper.

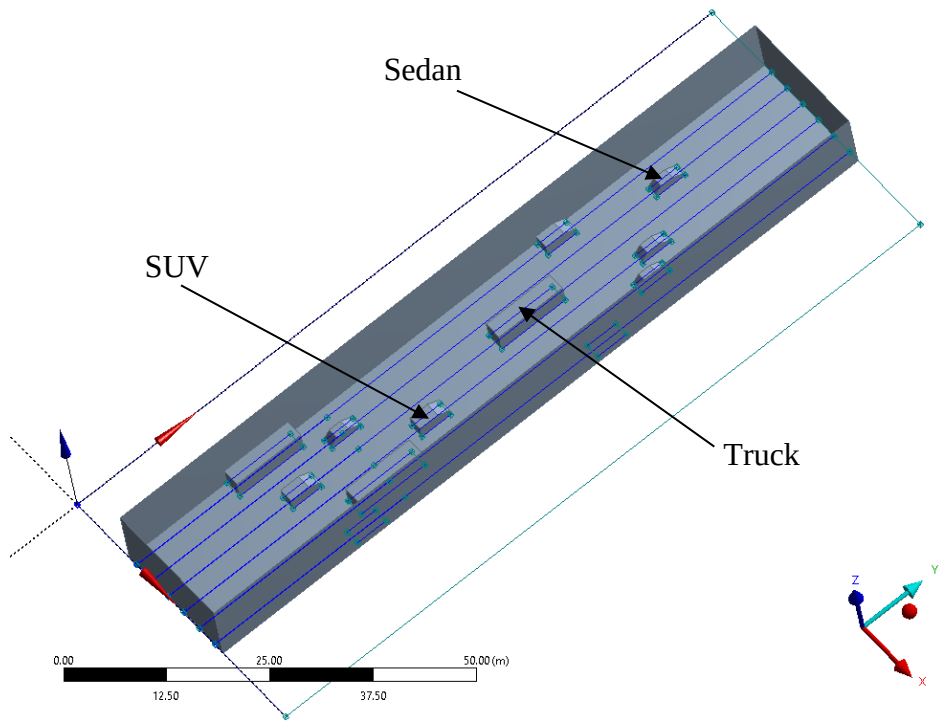

Figure 7. Geometry of vehicles

2.6 Numerical Settings

The SIMPLE (Semi-Implicit Method for Pressure Linked Equations) algorithm was used to solve the Navier-Stokes equations in the simulation. Second order upwind scheme was carried out for pressure, momentum, turbulent kinetic energy, turbulent dissipation rate, energy and species. The criteria were 10^{-3} for continuity, velocities and species, and 10^{-6} for energy. The time step size was 0.05 s to ensure stable simulation under the implicit scheme. The number of time steps was 20, and the maximum iteration in one single time step was 300 to assure enough iterations for solutions in each time step to be converged. The descriptions of boundary conditions are listed in Table 1.

Table 1. Boundary conditions

Name	Boundary	Description
Inlet	Velocity inlet	User-define function
Outlet	Outflow	Outflow with flow rate weighting = 1
Top	Symmetry	A zero flux of all quantities across a symmetry boundary
Side	Symmetry	A zero flux of all quantities across a symmetry boundary
Ground	Stationary wall	Roughness height: 0.01 m. Roughness constant: 0.5
Highway	Stationary wall	Roughness height: 0.001 m. Roughness constant: 0.5
Noise barrier	Stationary wall	Roughness height: 0. Roughness constant: 0.5
Vehicle	Stationary wall	Roughness height: 0. Roughness constant: 0.5
Exhaust	Velocity inlet	0.03, 0.04 and 0.05 m/s for sedans, SUVs and trucks [21]

3. RESULTS AND DISCUSSION

The results from numerical simulation were first completed by mesh independent study and validated with the wind tunnel experiment. The main results in this paper included noise barrier shape effects, influences of inflow conditions, automobile wakes and traffic flow effects. The representative automobile emission in this paper was carbon monoxide (CO). The whole numerical simulation domain was the mixture of carbon monoxide and air. The concentration of CO would have been expected to decrease if other automobile emission elements were included. All results were reflected in contours and vertical distribution of CO normalized concentration at different locations.

3.1 Mesh Independent Study

In order to obtain a mesh that could give reasonable results and efficient simulation, three sets of mesh were tested separately for noise barriers and traffic flow. Main simulation results, including velocity profiles and distribution of normalized concentration, were compared between different meshes.

3.1.1 Mesh for Noise Barrier Cases

Face sizing was inserted onto highway face and noise barrier surfaces. Different mesh size, thus, could be obtained by modifying the element size of mesh and face size. Table 2 lists the number of elements and nodes for each mesh. The smallest cell number means the coarsest mesh, and the largest cell number means the finest mesh.

Table 2. Mesh statistics

Mesh	Elements number	Nodes number
Mesh 1	298,818	57,017
Mesh 2	650,609	121,383
Mesh 3	820,942	153,706

Three sets of meshes for noise barriers were tested in this section. Results of velocity profiles and the vertical distribution of normalized concentration at x/H = 5 (5 times noise barrier height far

behind the barrier) were compared by using the three sets of meshes, as shown in Figure 8. The simulation results from mesh 2 and 3 were very close while those from mesh 1 deviated from the other two a little bit. The mesh with large amount of element could increase simulation accuracy, but it also prolonged computational time. Therefore, the medium mesh, mesh 2, was selected for later simulation, which brought a better balance in computational accuracy and the computing time.

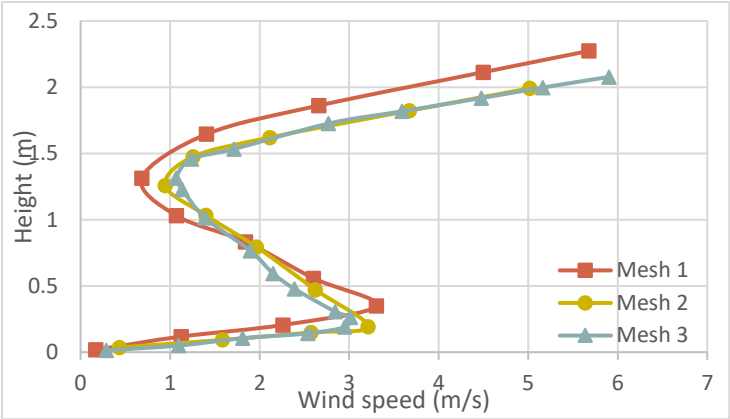

(a) Velocity profiles at x/H = 5

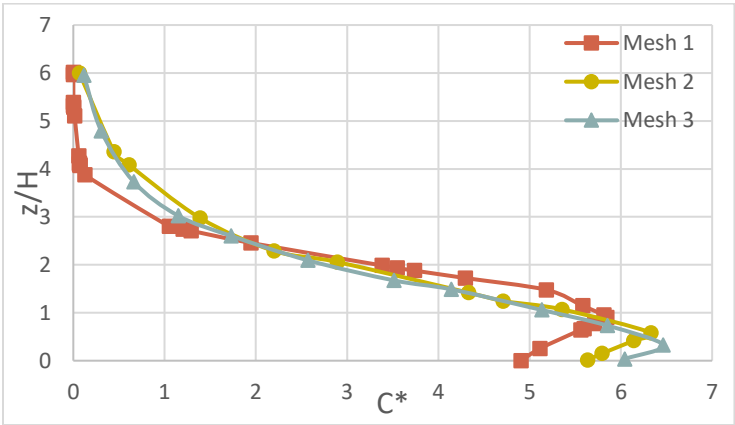

(b) Vertical distribution of normalized concentration at x/H = 5

Figure 8. Mesh independent study for noise barrier cases

Mesh 2 is shown in Figure 9. Figure 9 (a) is the close-up front view of the computational mesh and (b) is the close-up bottom view of the meshes around the noise barrier and highway. The clustered meshes around the noise barrier and highway can be seen clearly, which can solve the flow features accurately near the highway and noise barrier.

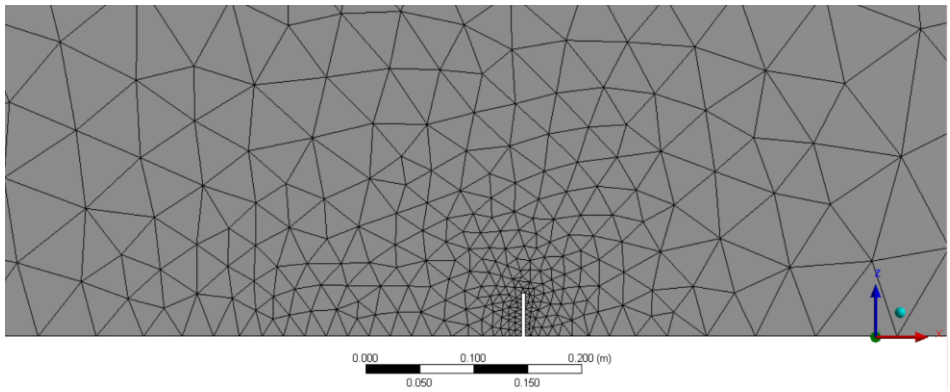

(a) Close-up front view

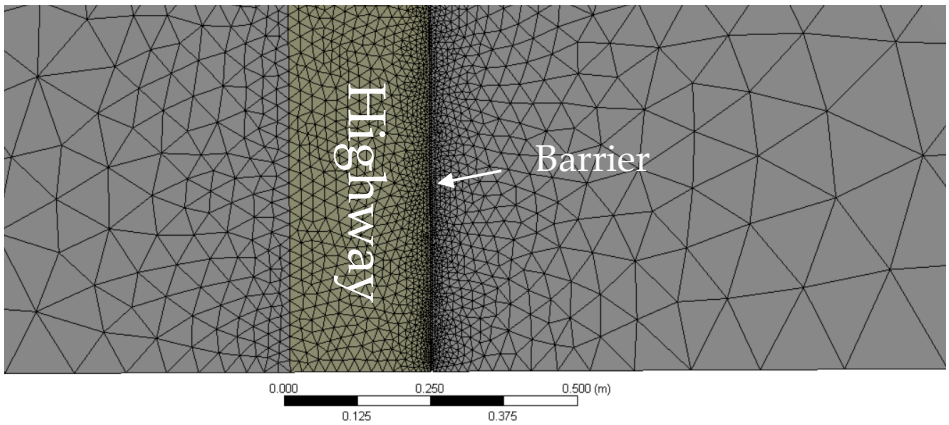

(b) Close-up bottom view

Figure 9. View of mesh 2

3.1.2 Mesh for Traffic Flow Cases

Three sets of mesh density were implemented in a small computational domain created for the highway. The mesh inflation was inserted on the entire bottom face to accurately capture the boundary layer features of turbulent flows. The maximum layers were 5, and the growth rate was 1.2. The mesh body sizing was applied on the small computational domain, and the mesh face sizing was applied on all vehicles in the domain. Three meshes were generated by changing the body and face size, as listed in Table 3.

Table 3. Mesh statistics

Mesh	Elements number	Nodes number
Mesh 1	172,268	41,471
Mesh 2	187,932	44,731
Mesh 3	287,080	63,722

Velocity profiles and vertical distribution of normalized concentration at the center of the highway that were solved by three different meshes were compared in Figure 10.

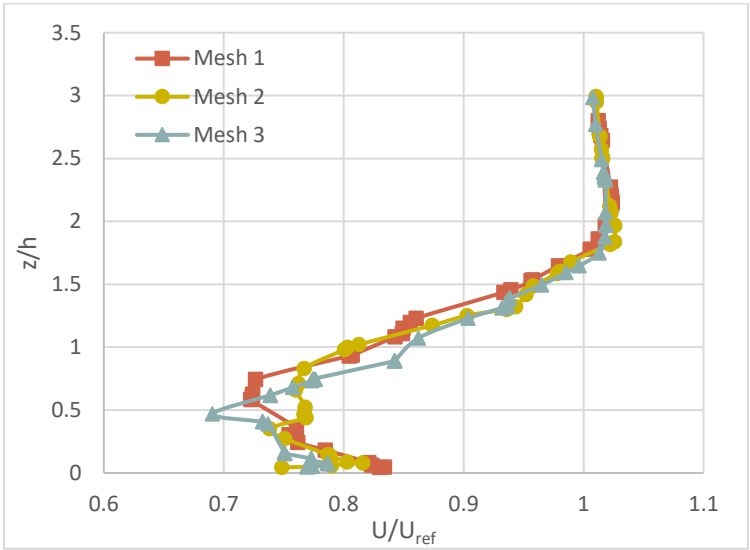

(a) Velocity profiles at the center of the highway

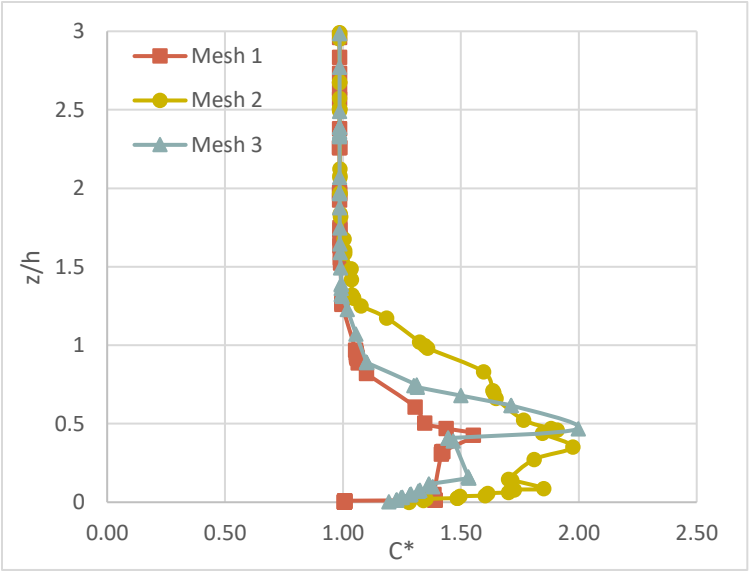

(b) Vertical distribution of normalized concentration at center of the highway

Figure 10. Mesh independent study for traffic flow cases

As shown in Figure 10, three sets of meshes could give similar results for the velocity profile and the emissions dispersion. There were only a few changes at some points between mesh 2 and 3. Mesh 1 could also give approximate results even with less nodes and elements. One of the very apparent differences was the maximum normalized concentration: approximately 1.5 for mesh 1

while 2.0 for mesh 2 and 3. Generally, finer mesh can give more accurate results but cost more computational time and storage. As a result, mesh 2, which brought a better balance in computational accuracy and efficiency, was used for simulation for traffic flow in this paper. A full view of mesh is shown in Figure 11.

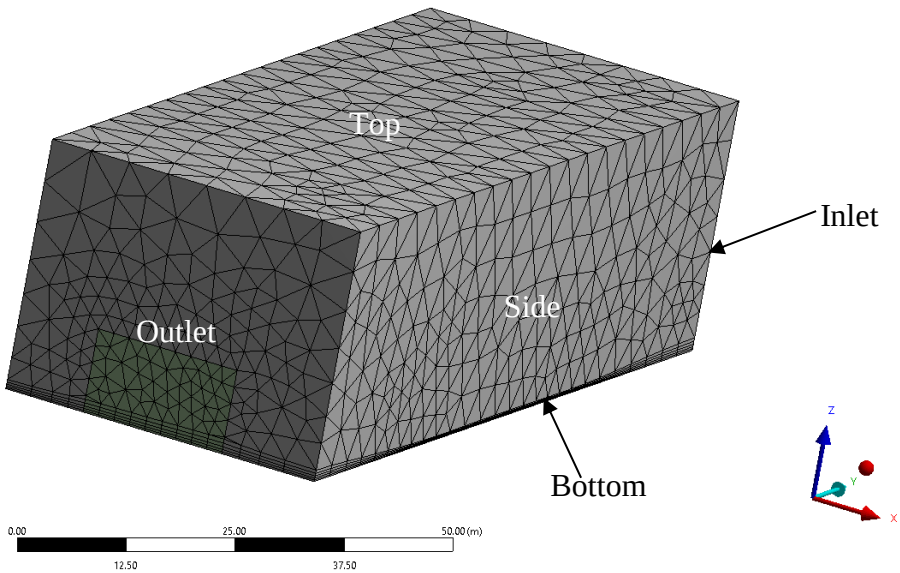

Figure 11. View of mesh 2

3.2 Model Validation with Wind Tunnel Experiment

In this section, validation was done separately for noise barriers and traffic flow due to different wind tunnel experiments. Turbulence models and species models were validated with those wind tunnel experiments by comparing wind profiles and the vertical distribution of the normalized emission concentration.

3.2.1 Validation for Noise Barrier Cases

The reference configuration in the wind tunnel experiment was a flat highway along with a single 6-meter-high rectangular noise barrier. The non-reaction species transport model was the only species model to be applied because this study only considered the transportation of emissions in the computational domain. All simulation results obtained by turbulence models were compared with the wind tunnel experiment data, as shown in Figure 12.

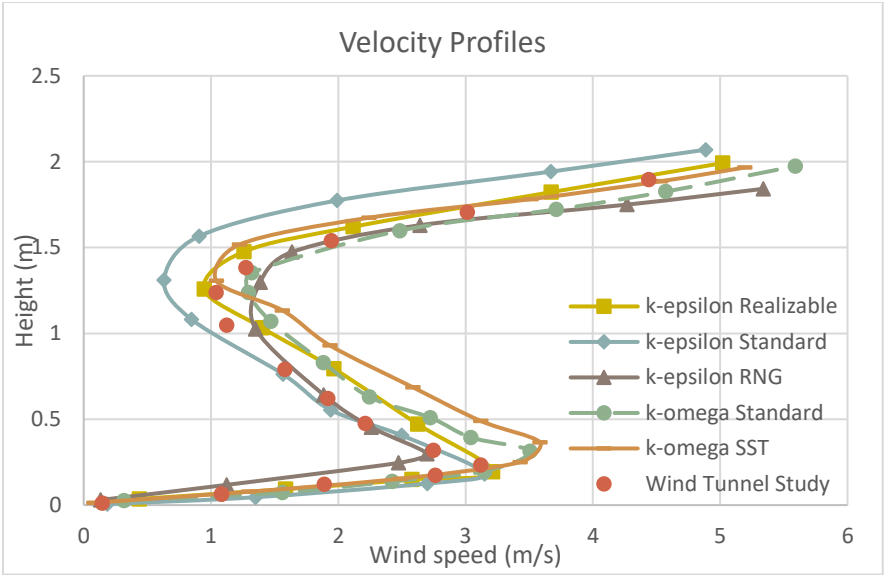

(a) Velocity profiles at x/H = 5

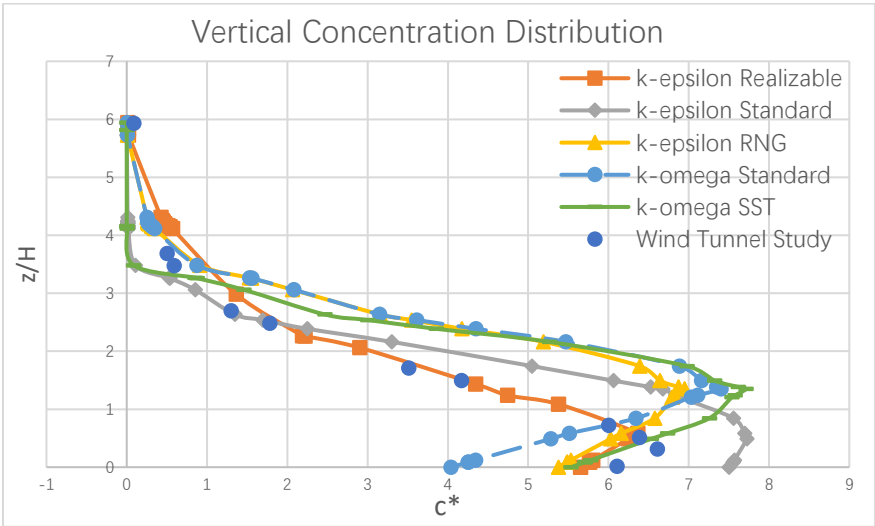

(b) Vertical distribution of C_2H_6 normalized concentration at x/H = 5

Figure 12. Model comparison and validation

In Figure 12 (a), the biggest differences between each model were at two turning points where the realizable k-ε model matched better with the wind tunnel study. In Figure 12 (b), all turbulence models matched well with the wind tunnel study in the high altitude ($z/H \geq 3$; higher than 3 times noise barrier height). However, in the near-ground region ($z/H \leq 3$), the result for each turbulence model varied a lot. This study focused more on the near-ground region because there are many communities and buildings that are located near highways. Under z/H = 3, the realizable k-ε model

matched better with the wind tunnel study. Consequently, the realizable k-ε model was used in the following simulation.

3.2.2 Validation for Traffic Flow Cases

Velocity profiles at two locations behind the vehicle model were compared between simulation results and experimental data, as shown in Figure 13. The distance from the vehicle was normalized by the vehicle height. The simulation results were solved by different k-ε model: standard k-ε model, realizable k-ε model and RNG k-ε model. The horizontal axis is dimensionless wind speed, which is normalized by the reference wind speed, 2.5 m/s in this case. The vertical axis is dimensionless height that is normalized by the vehicle height.

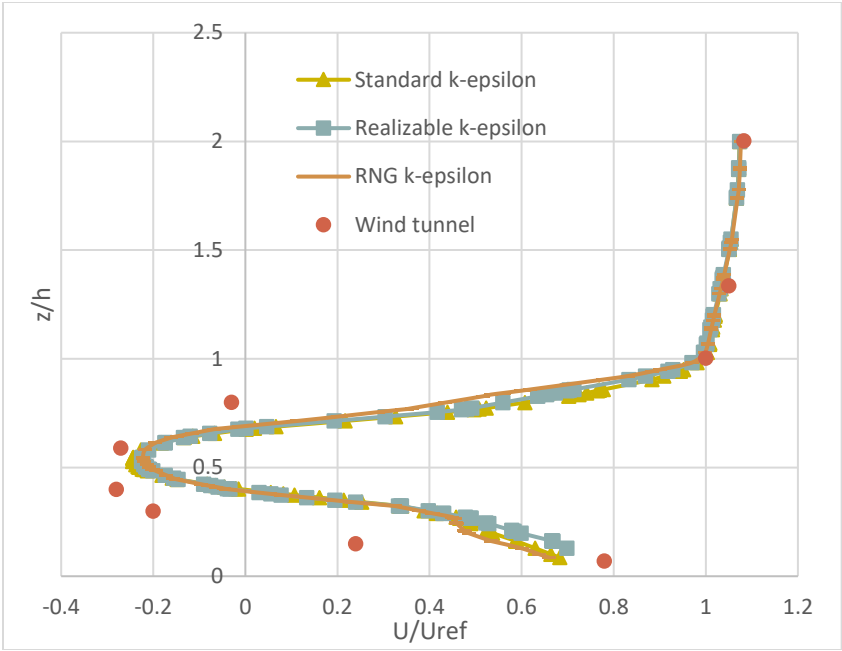

(a)Velocity profiles at x/h = 0.4

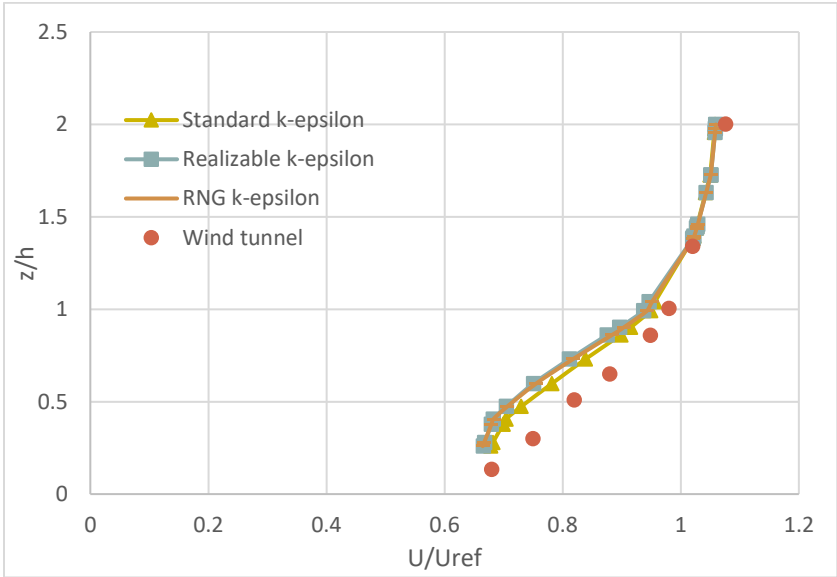

(b) Velocity profiles at x/h = 7.47

Figure 13. Comparison of velocity profiles

Figure 13 (a) showed the vertical wind profile at a location nearly behind the car while Figure 13 (b) showed that at a location far behind the car. In Figure 13 (a), negative velocity occurred behind the car, indicating the reverse flow and recirculation in automobile wake regions. In Figure 13 (b), as the downstream distance is far enough, the wind profile recovered to the power law relation. For both locations, all k-ε models matched well with the wind tunnel experimental data;

nevertheless, during the computation, the RNG k-ε model took much more time to obtain a converged solution. Therefore, the standard k-ε model was adopted in the following simulation for traffic flow because of the computational efficiency and reasonable accuracy.

To validate the species model, the vertical distribution of normalized emission concentration was compared with the wind tunnel data at two locations behind the vehicle. The comparison is shown in Figure 14. The vertical distance was normalized by the vehicle height. The concentration was normalized by a product of reference velocity, vehicle height and volumetric flow rate of the emission.

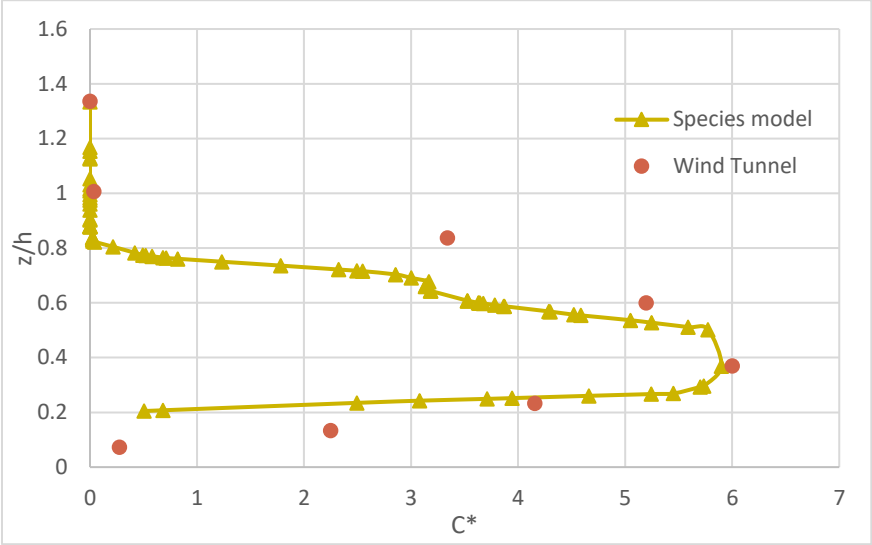

(a) Vertical distribution of normalized concentration at x/h = 0.44

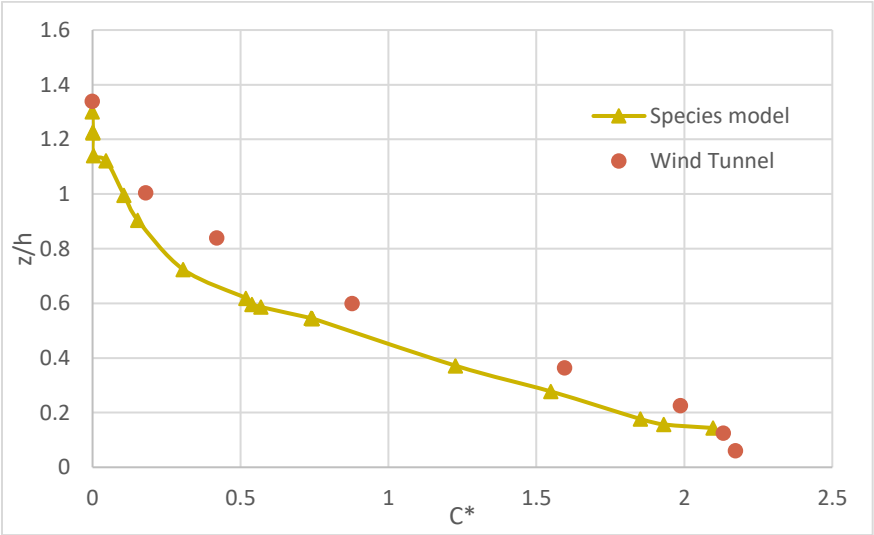

(b) Vertical distribution of normalized concentration at x/h = 3.8

Figure 14. Comparison of vertical distribution of C_3H_8 normalized concentration

Figure 14 (a) showed the vertical distribution of emissions near behind the car. The maximum emissions concentration appeared about the half height of the car, which was a little above the spot of the tailpipe. In Figure 14 (b), the concentration simply dissipated along with the height at a place far from the car. Through the comparison in Figure 14, similar trend was observed for both locations; consequently, the species model was considered as valid.

3.3 Noise Barrier Shape Effects

This section studied the noise barrier shape effects on the dispersion of automobile emissions. Different shapes of noise barrier were classified by their cross-sectional geometry. Rectangular and T-shaped noise barriers were tested in this paper. Their full-scale dimensions were shown in Figure 15.

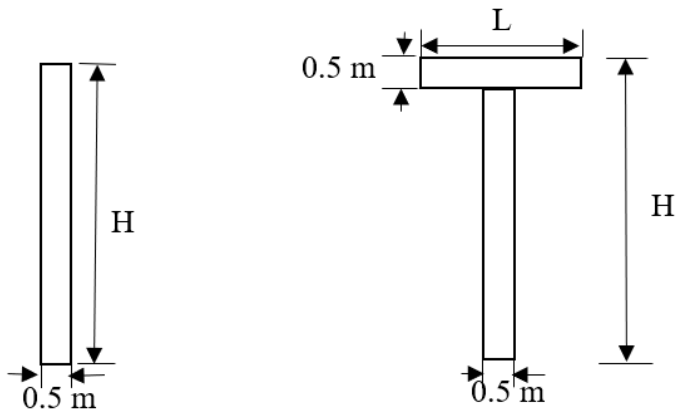

(a) Rectangular (b) T-shaped

Figure 15. Cross-sections of different noise barrier shapes

In the computational domain, however, the noise barriers became 1:150 scaled models as the wind tunnel in the validation also used scaled models. The rectangular and the T-shaped noise barrier were separately created along the highway on the downstream side in the computation domain, as shown in Figure 16.

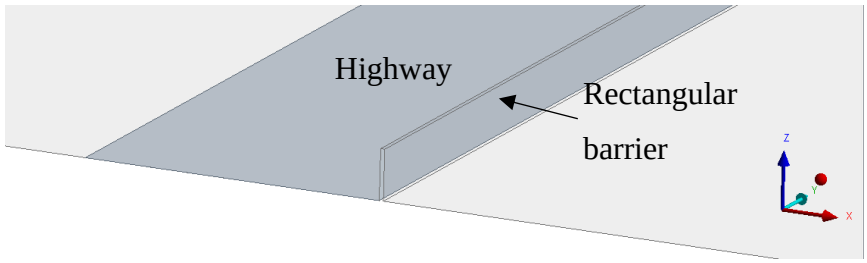

(a) Rectangular noise barrier

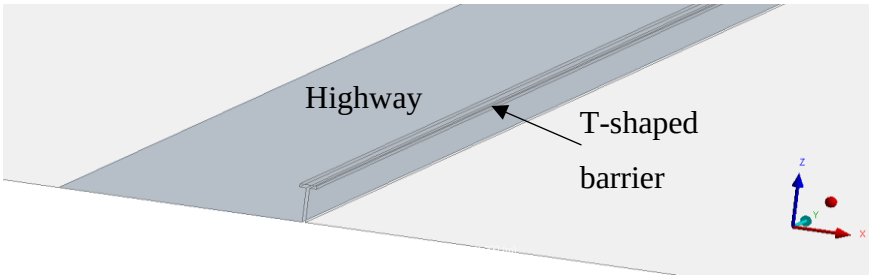

(b) T-shaped noise barrier

Figure 16. Noise barrier in the computational domain

The rectangular noise barrier has one critical parameter, i.e. height H. The T-shaped noise barrier, however, has an additional important parameter, i.e. top length L. For T-shaped noise barriers, a ratio of the top length to the height, L/H, becomes a dimensionless parameter. In order to study the noise barrier shape effects, one rectangular and four T-shaped and noise barriers were tested respectively. The details of each noise barrier are listed in Table 4. The thickness of the noise barrier in all simulation cases is 0.5 m in the full scale.

Table 4. Dimensions of noise barriers

Simulation Case	Barrier Type	Dimensions
Base case	Rectangular	H = 6 m
Case 1	T-shaped	H = 6 m, L = 1.0 m (L/H = 0.167)
Case 2	T-shaped	H = 6 m, L = 1.5 m (L/H = 0.250)
Case 3	T-shaped	H = 6 m, L = 2.0 m (L/H = 0.333)
Case 4	T-shaped	H = 6 m, L = 2.5 m (L/H = 0.417)

Carbon monoxide (CO) was used to represent the automobile emissions. Five cases listed in table 4 were simulated by using realizable k-ε model and non-reaction species transport model. The contours of CO molar concentration on the symmetry plane of the computational domain are shown below in Figure 17.

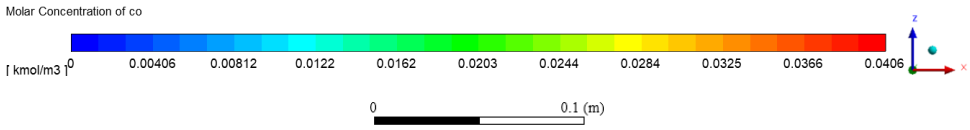

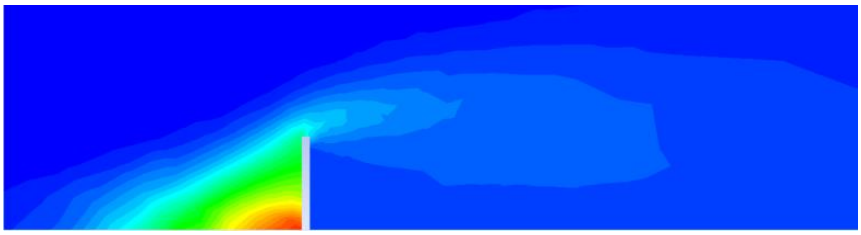

(a) Base case

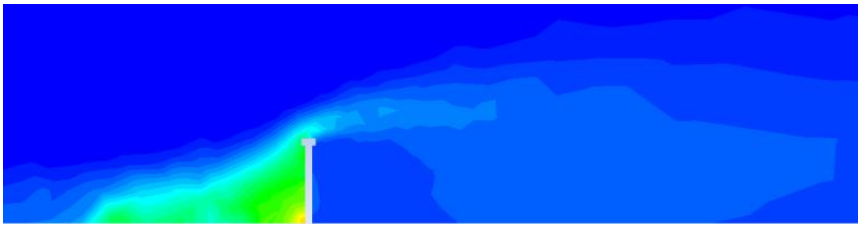

(b) Case 1

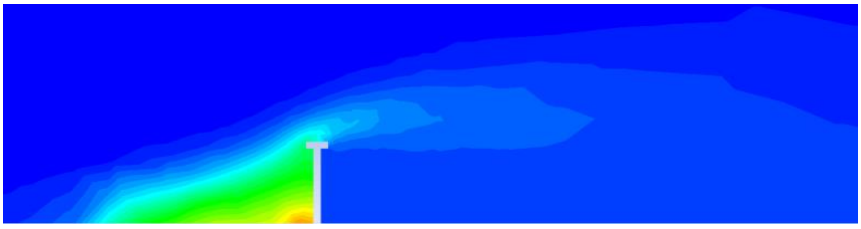

(c) Case 2

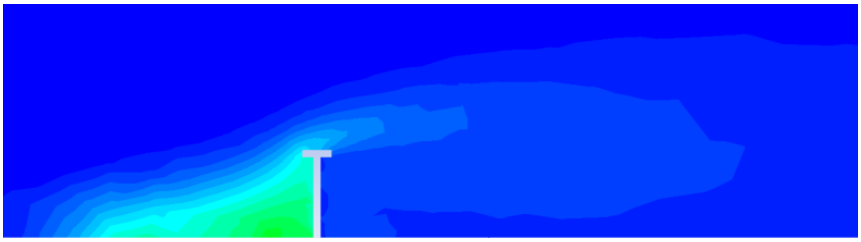

(d) Case 3

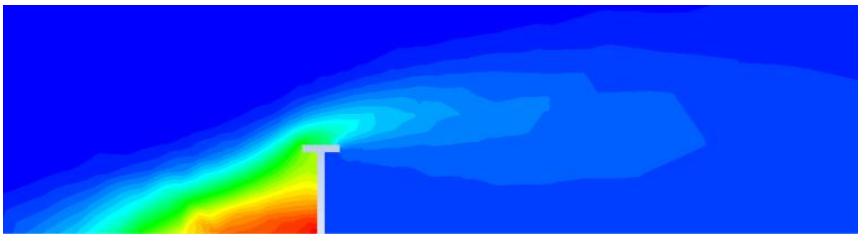

(e) Case 4

Figure 17. Contours of CO molar concentration for different noise barrier shapes (H = 6 m)

It was illustrated in Figure 17 that not all four types of the T-shaped noise barriers were able to significantly mitigate the downstream emission relative to the rectangular noise barrier. The performance was highly related to the noise barrier shape. T-shaped noise barriers with different top length had great differences. As expected, highway noise barriers could reduce the downstream emission concentration while much emission was trapped on the highway. The T-shaped noise barriers in case 1, 2, and 3 had better performance than the rectangular and the T-shaped barrier in case 4 because they had less concentration both downstream and on the highway. However, case 4 suggested that such a long cap length for the T-shaped didn't influence too much on the downstream emission compared to the base case. On the contrary, it gathered a little more concentration on the highway by its long cap.

Next, Figure 18 compares the vertical distribution of normalized concentration between each case at four locations: x/H = 0 (center of the highway), x/H =5, x/H = 10 (near the highway), and x/H= 50 (far downstream). Each line in one plot recorded how much emissions from the ground (z = 0) to the height where the normalized concentration of emissions became zero.

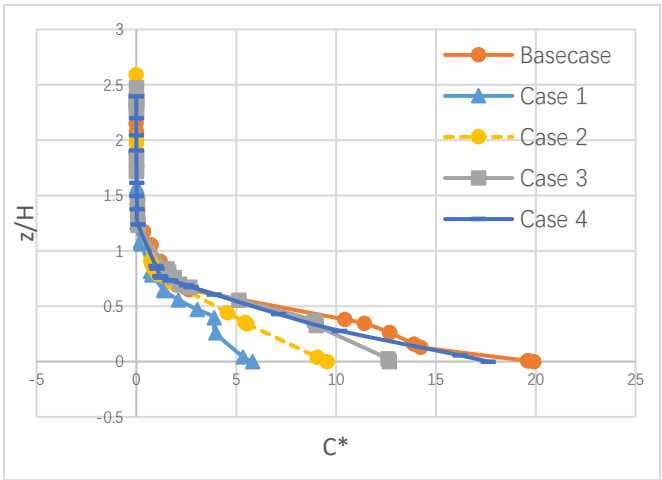

(a) Vertical distribution of normalized concentration at x/H = 0

Figure 18. Vertical distribution of normalized concentration at different locations (H = 6 m)

Figure 18 continued

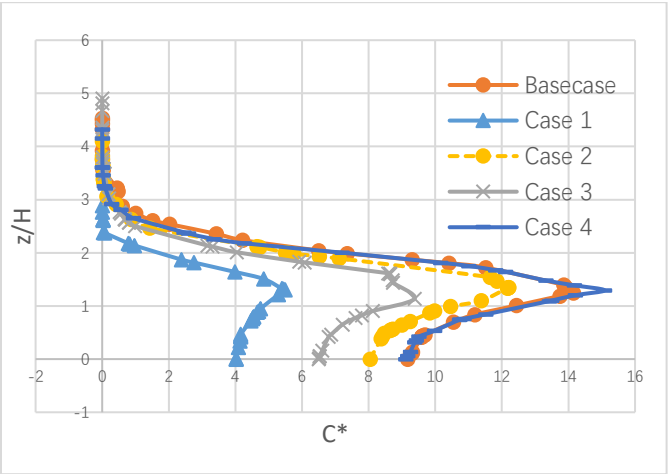

(b) Vertical distribution of normalized concentration at x/H = 5

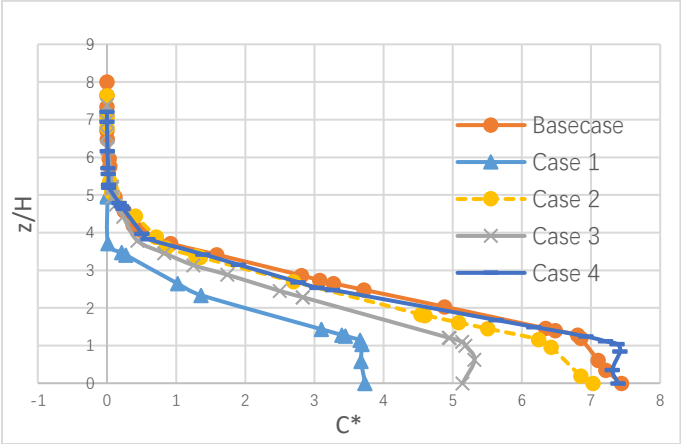

(c) Vertical distribution of normalized concentration at x/H = 10

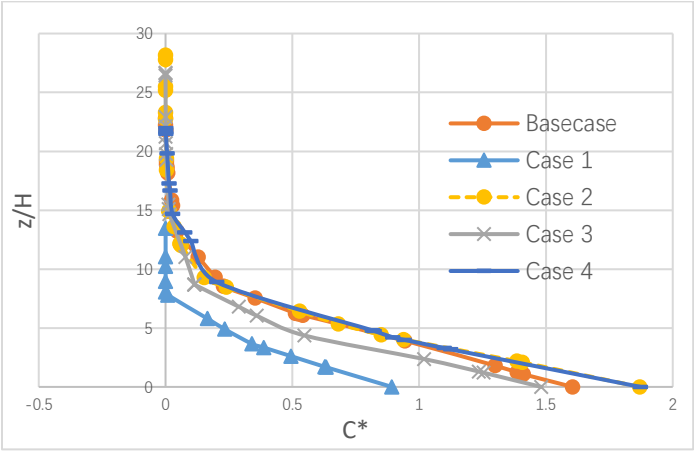

(d) Vertical distribution of normalized concentration at x/H = 50

The horizontal axis in Figure 18 is the normalized concentration. The value of the normalized concentration decreased from the location x/H = 0 to 50. It implied that the emission was mostly on the highway and became less and less at further downstream regions. The vertical axis in Figure 18 is the ratio of height to the noise barrier height (z/H), which is also dimensionless. It was clearly demonstrated that the near-ground region always had more emission than that at higher altitude regions except the location at x/H = 5 because there were still a lot of emissions flowing downstream in the air and not completely settled on the ground.

The locations, x/H = 5 and 10, were areas relatively close to the highway. At these two locations, the base case and case 2 and 4 had similar vertical concentration distribution, but case 1 showed less concentration in the near-ground region. For the far downstream region, x/H = 50, all cases gave similar results because the influence of noise barriers had less influence in such far area, although case 1 was able to mitigate more emissions.

All contours illustrated that noise barriers could reduce emissions concentration in the downstream area, but much emissions would be trapped on the highway, especially in the lower corner of the noise barrier. The further downstream the lower concentration in the near-ground region. For all four locations, case 1 appeared to have the best performance. It can be concluded that T-shaped noise barriers can help reduce more emissions downstream than rectangular ones. However, a few of T-shaped barriers had similar results while others varied a little bit. The results highly depended on the top length of T-shaped barriers. Therefore, the further study was to increase the noise barrier height because the top length could not keep increasing for one height in the real situation.

In the following, all five cases with H = 9 m (full scale) noise barrier were studied again. Different height, for T-shaped noise barriers, would change the ratio of the top length to the height (Table 5), so it implicitly gave more available top lengths in addition to the previous simulation if the stability for the T-shaped structure had to be considered.

Table 5. More available ratios for T-shaped noise barriers

Simulation Case	Barrier Type	Dimensions
Base case	Rectangular	H = 9 m
Case 1	T-shaped	H = 9 m, L = 1.0 m (L/H = 0.111)
Case 2	T-shaped	H = 9 m, L = 1.5 m (L/H = 0.167)
Case 3	T-shaped	H = 9 m, L = 2.0 m (L/H = 0.222)
Case 4	T-shaped	H = 9 m, L = 2.5 m (L/H = 0.278)

Similarly, comparisons between contours and plots of concentration distributions were shown in Figure 19 and 20, respectively.

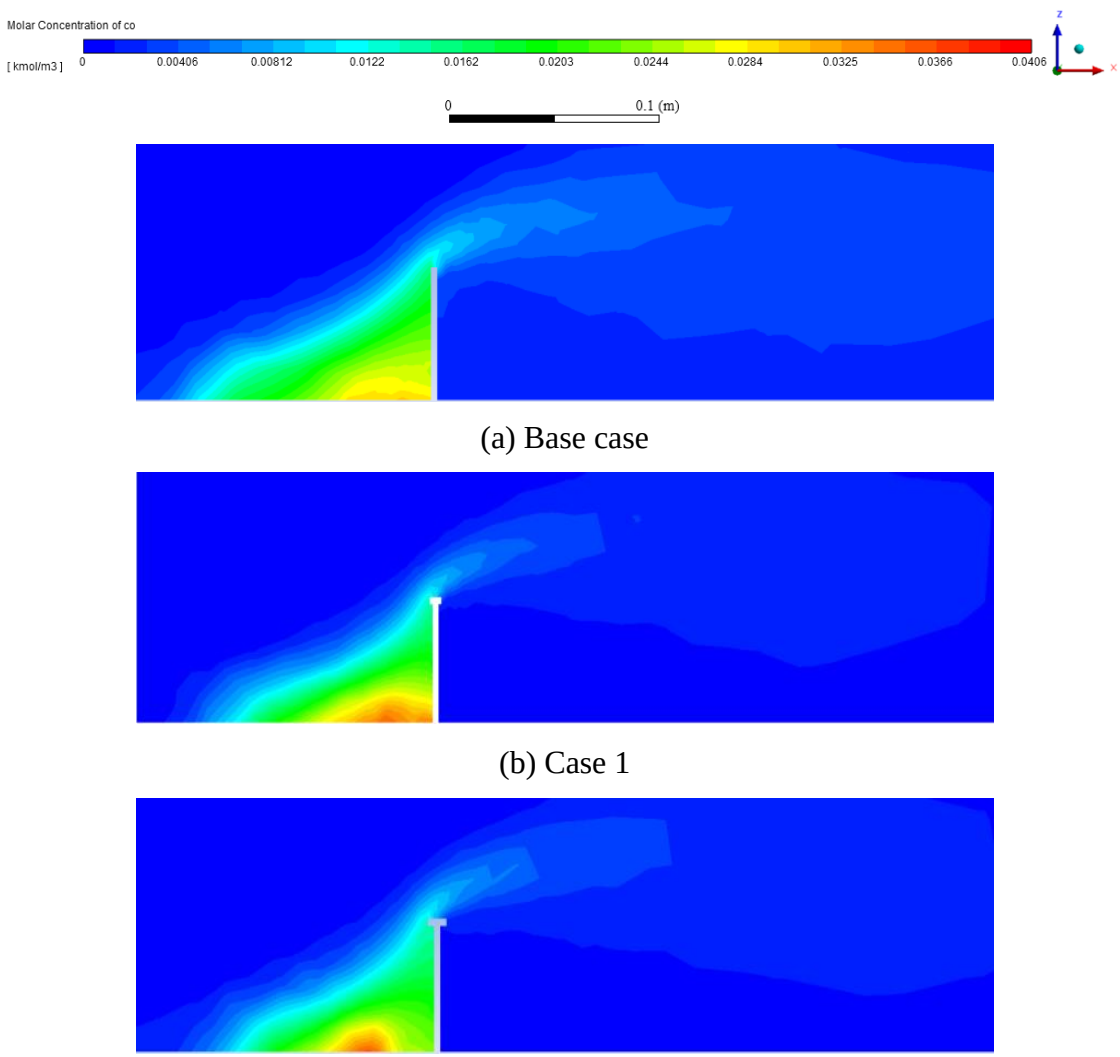

(a) Base case

(b) Case 1

(c) Case 2

Figure 19. Contours of CO molar concentraiton for different noise barrier shapes (H = 9 m)

Figure 19 continued

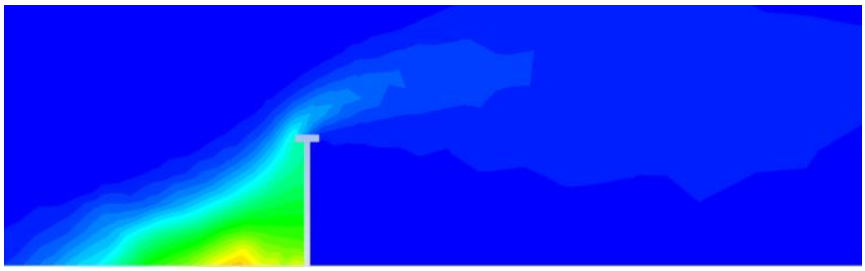

(d) Case 3

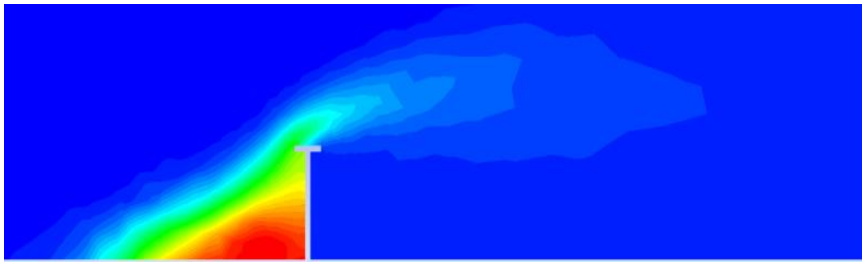

(e) Case 4

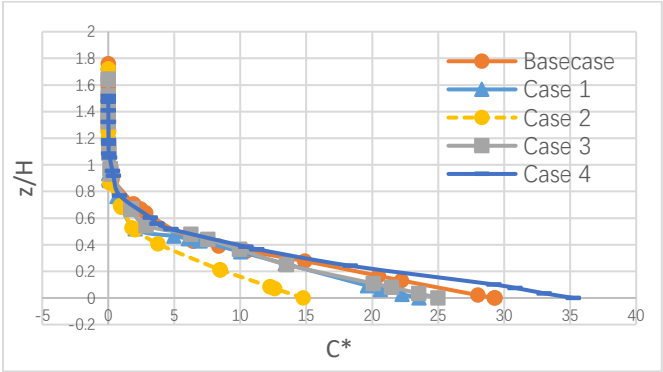

(a) Vertical distribution of normalized concentration at x/H = 0

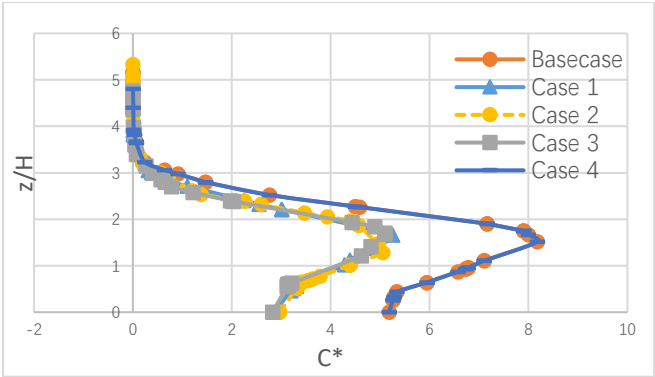

(b) Vertical distribution of normalized concentration at x/H = 5

Figure 20. Vertical distribution of normalized concentration at different locations (H = 9 m)

Figure 20 continued

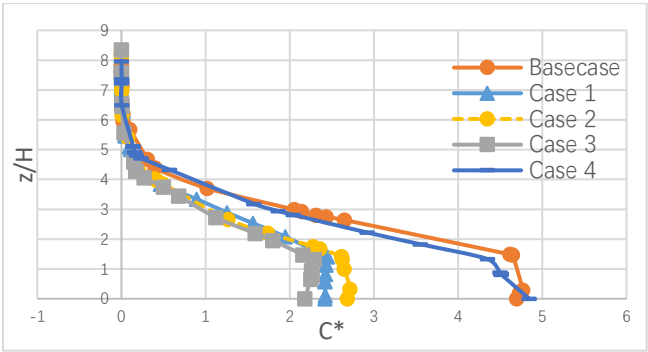

(c) Vertical distribution of normalized concentration at x/H = 10

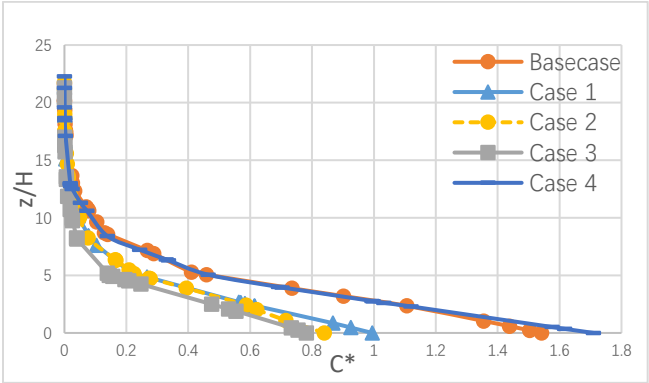

(d) Vertical distribution of normalized concentration at x/H = 50

The contours and plots in Figure 19 and 20 showed similar patterns to the previous simulation. One noticeable point was that more emissions were trapped on the highway and that less emissions were distributed in downstream regions, so increasing noise barrier height could reduce more downstream emissions. In Figure 20 (a), case 2 had the best performance for the emission on the highway with the lowest emission concentration; in the downstream regions, from Figure 20 (b) (c) and (d), case 3 appeared to be the best one despite case 1 and 2 were also relatively good. Again, it proved that a few T-shaped noise barriers would have similar results as suggested from the previous simulation. This could be explained by the fact that the top length would need to be accordingly longer if the T-shaped noise barrier has higher height so that an optimized ratio of the top length to the height could be satisfied.

As a result, the best cases in this study were case 1 for 6 m high T-shaped noise barrier and case 2 for 9 m high T-shaped noise barrier on the highway and case 3 for 9 m high T-shaped noise barrier

in the downstream region. For T-shaped noise barriers, an optimized ratio of the top length to the barrier height could range roughly from 0.17 to 0.22.

3.4 Influence of Inflow Conditions

In this section, the influence of inflow conditions on the dispersion of automobile emissions was studied in addition to different shapes of noise barriers. Three different inflow conditions were compared: uniform inflow, linear approximation to the power law, and the power law. Different inflow conditions distinguish whether or not one would create wind shear. The uniform inflow condition has a constant wind speed, so there is no velocity difference thereby no wind shear. The linear approximation describes that the wind speed has a linear correlation to the height, so it creates constant wind shear. The power law describes that the wind speed varies with height exponentially, and the wind shear along with turbulence and vorticity varies with height as well.

3.4.1 Uniform Inflow

The uniform inflow condition had a constant wind speed at 7 m/s. Five simulation cases with 6-meter-high noise barrier (full scale) were solved under the uniform inflow condition. The vertical distribution of CO normalized concentration was shown in Figure 21.

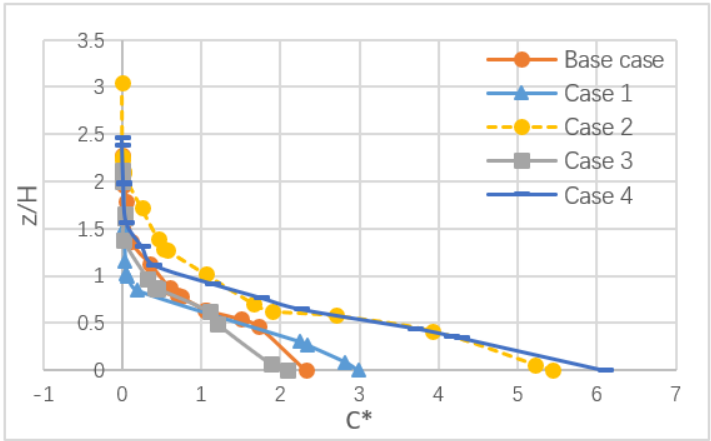

(a) Vertical distribution of normalized concentration at x/H = 0

Figure 21. Vertical distribution of normalized concentration at different locations

Figure 21 continued

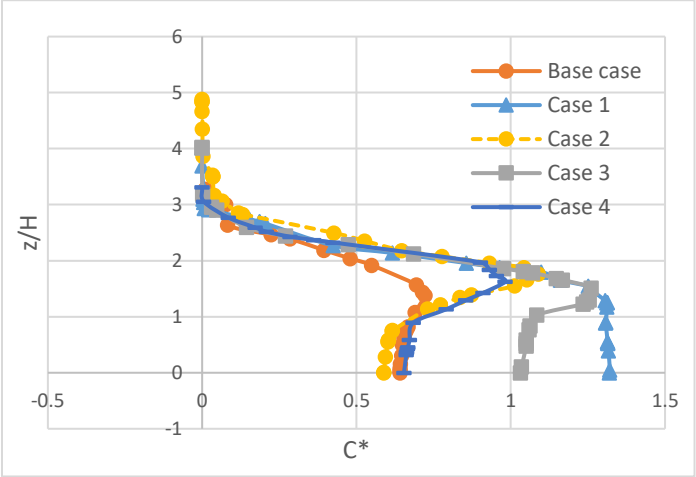

(b) Vertical distribution of normalized concentration at x/H = 5

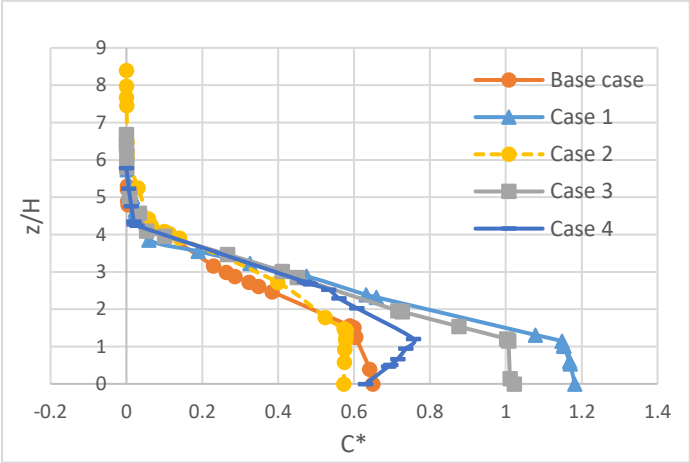

(c) Vertical distribution of normalized concentration at x/H = 10

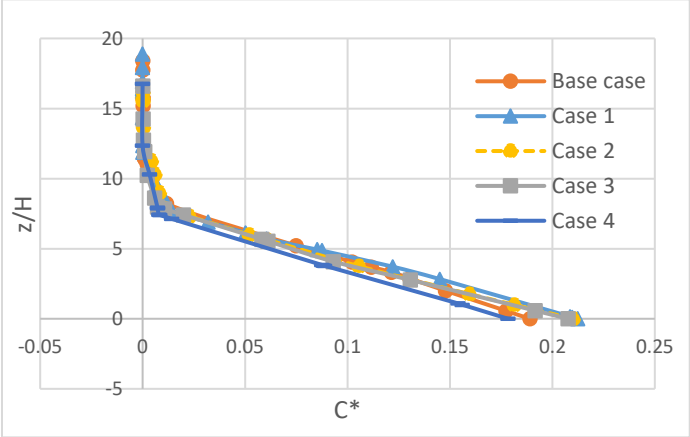

(d) Vertical distribution of normalized concentration at x/H = 50

Under the uniform inflow condition, the base case, case 1 and 3 appeared to have similar performance on the highway; meanwhile, case 2 and 4 also had similar results. In the near-highway regions, the base case and case 2 turned to be comparable cases and became relatively better cases under the uniform inflow condition. In the far downstream area, the CO concentration would become very light, so there was not big difference between each case. As a matter of fact, the shape effects of noise barrier would become insignificant in the far downstream area.

3.4.2 Linear Approximation

The linear approximation proposed that the wind speed correlated with height linearly. As constant velocity difference existed in an increment of height, the wind shear was present in this inflow condition. The vertical distribution of CO normalized concentration was shown in Figure 22.

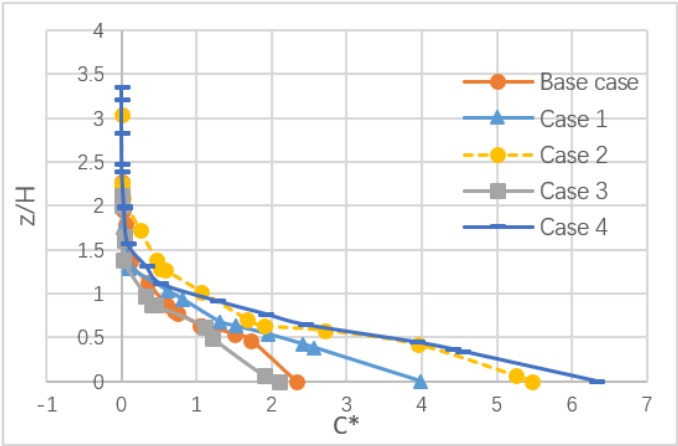

(a) Vertical distribution of normalized concentration at x/H = 0

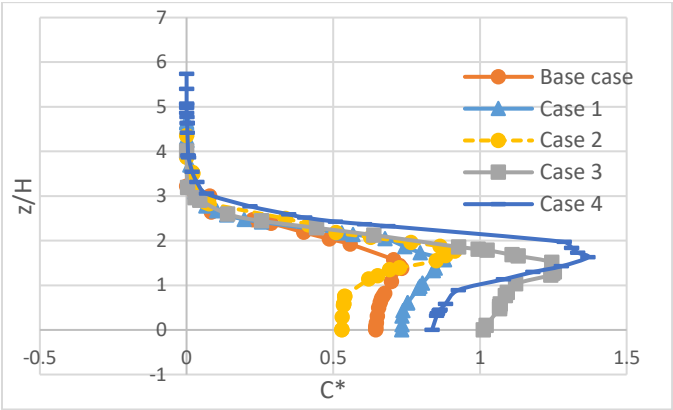

(b) Vertical distribution of normalized concentration at x/H = 5

Figure 22. Vertical distribution of normalized concentration at different locations

Figure 22 continued

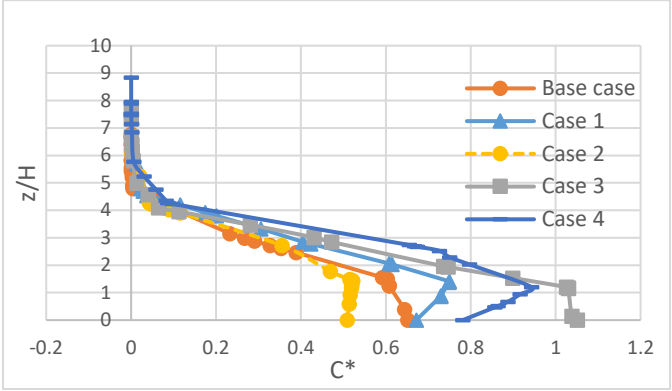

(c) Vertical distribution of normalized concentration at x/H = 10

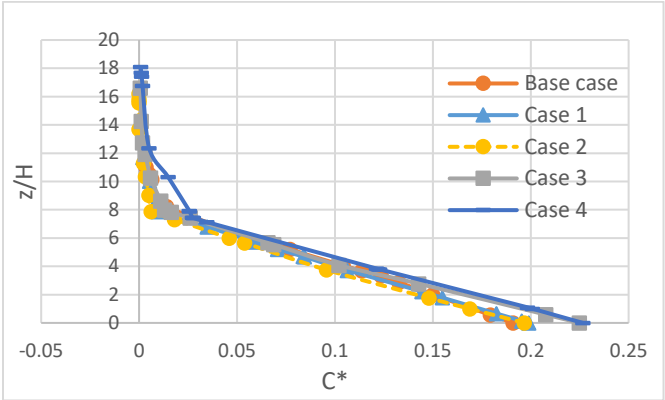

(d) Vertical distribution of normalized concentration at x/H = 50

Under the linear inflow condition, unlike the uniform inflow condition, the results of five cases varied a lot in the near-highway regions in Figure 22 (b) and (c). That could be explained with the existence of wind shear. Linear inflow would create wind shear that could contribute to the transportation and dissipation of highway emissions. Case 3 showed least concentration on the highway (x/H = 0) while case 2 was in a better condition for near-highway regions (x/H = 5, 10). However, the level of emission reduction by the T-shaped was not critical compared to the base case results. Likewise, all cases had very similar results in the far downstream area (x/H = 50) because the shape effects of noise barrier became insignificant.

3.4.3 Power Law

The power law suggested that the wind speed correlated with height exponentially; consequently, large velocity difference existed in this inflow condition. The wind shear along with turbulence

was expected to create. The vertical distribution of CO normalized concentration was shown in Figure 23.

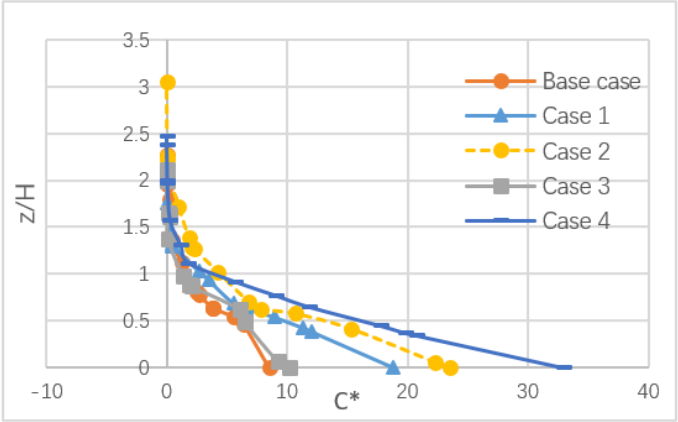

(a) Vertical distribution of normalized concentration at x/H = 0

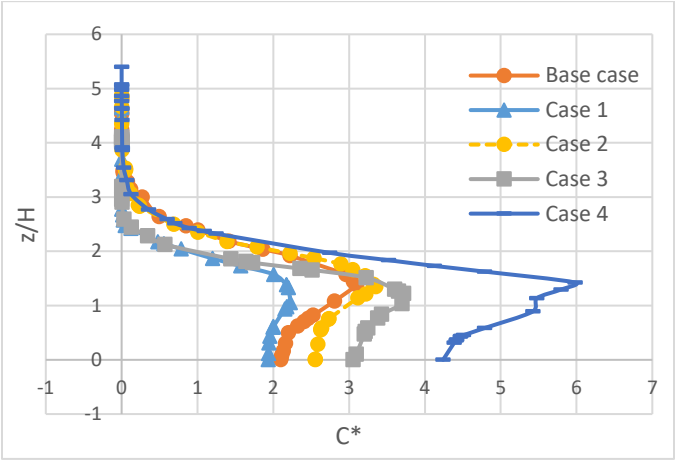

(b) Vertical distribution of normalized concentration at x/H = 5

Figure 23. Vertical distribution of normalized concentration at different locations

Figure 23 continued

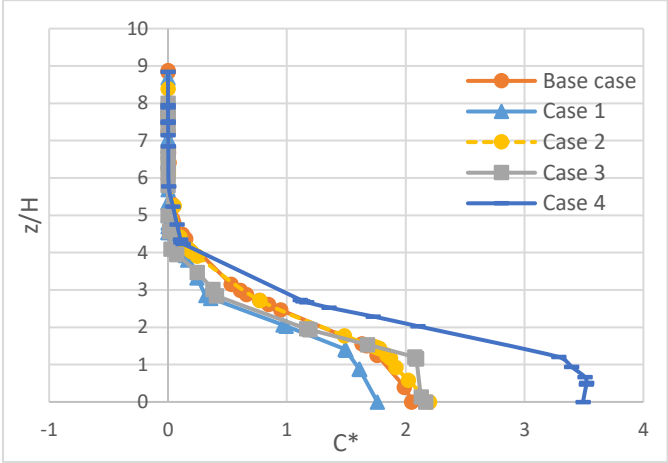

(c) Vertical distribution of normalized concentration at x/H = 10

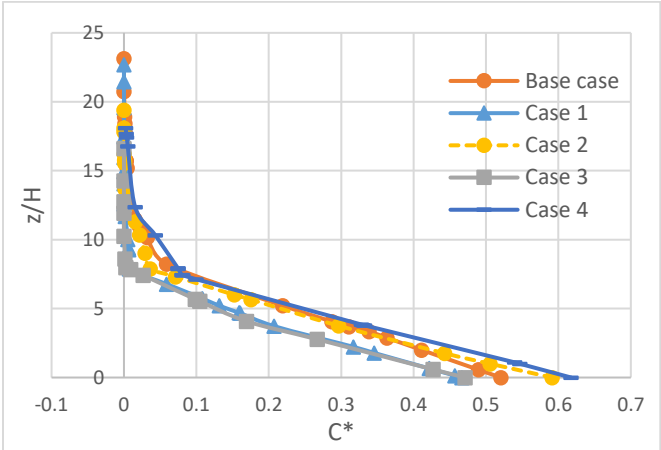

(d) Vertical distribution of normalized concentration at x/H = 50

Compared with last two inflow conditions, the power law profile brought much more emissions to downstream regions because the exceptional wind shear and turbulence under the power law could truly stimulate the transportation and the dispersion of automobile emissions on the highway. For the near-highway regions, Figure 23 (b) and (c), case 1 was still the best case under the power law even though the reference velocity and height were different for this simulation. However, it was unable to have dramatic reduction on CO concentration, especially in the far downstream area where case 1 illustrated similar results with other cases.

In summary, noise barrier shapes could make differences to the dispersion of automobile emissions in downstream regions. T-shaped noise barriers performed better than rectangular ones on reducing

downstream emissions concentration. However, the noise barrier shape effects were also highly influenced by inflow conditions. A few noise barriers would manifest similar results even though they had different shapes. The noise barrier shape effects could become significant under certain inflow conditions.

3.5 Automobile Wake Effects

From this section, moderate traffic flow was added on the highway in a full scale. This section reported the automobile wake effects on the dispersion of emissions on the highway. Automobile wakes are inevitably present behind fast-moving vehicles on the highway. Turbulence and recirculation are supposed to occur in automobile wakes. Exhausts are always emitted backwards, so it brings much interest that wakes behind vehicles would affect the dispersion of emissions. Major results included velocity fields on each lane and the vertical distribution of CO normalized concentration at different locations of the highway with and without noise barriers.

There were six lanes on the highway and two vehicles on each lane. Figure 24 shows velocity streamlines on the central plane of each lane for the case without noise barriers.

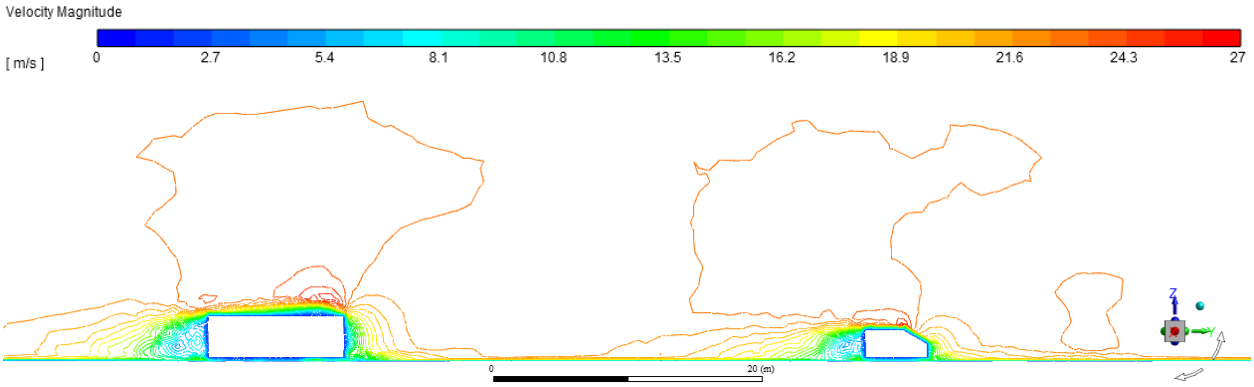

(a)

Figure 24. Velocity streamlines without noise barriers on (a) – (f) six lanes

Figure 24 continued

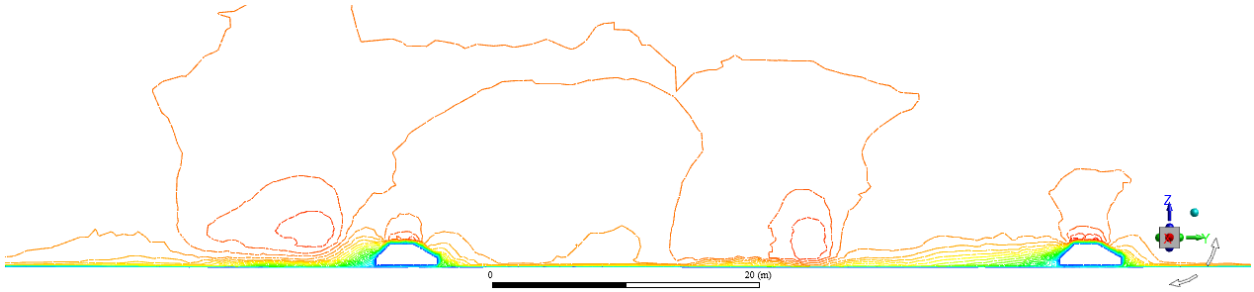

(b)

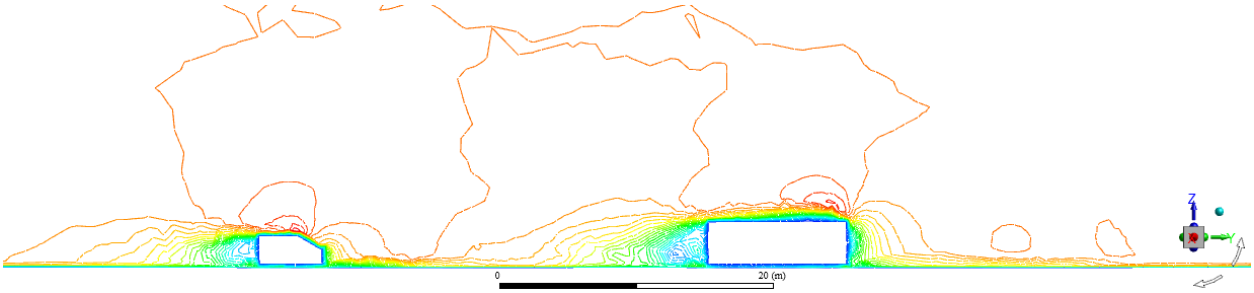

(c)

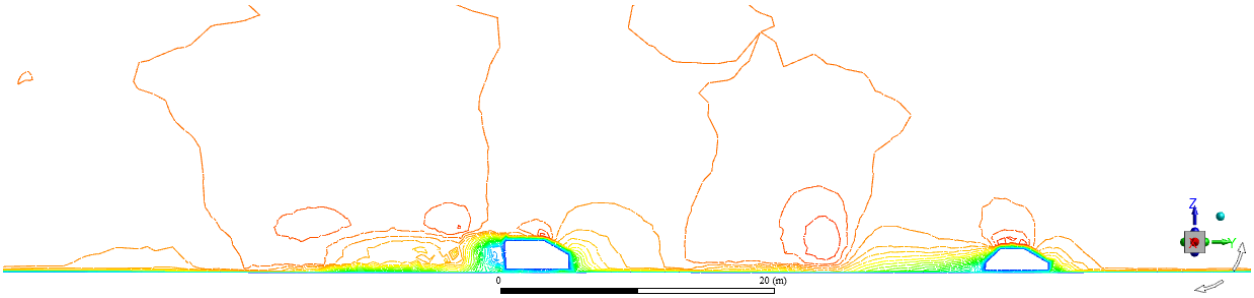

(d)

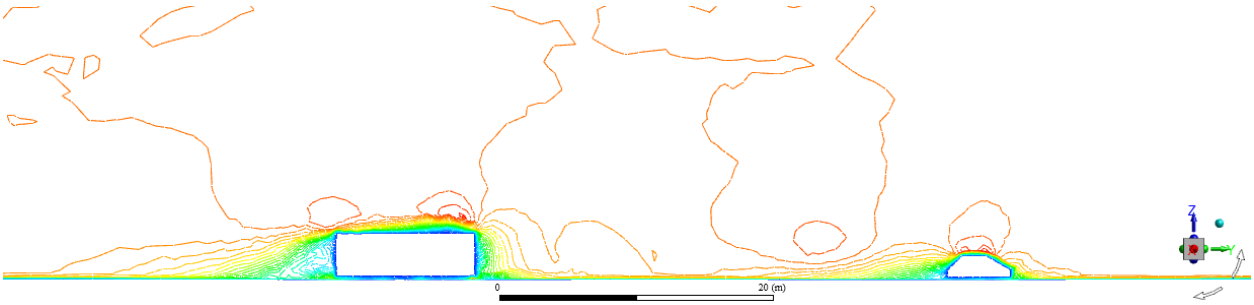

(e)

Figure 24 continued

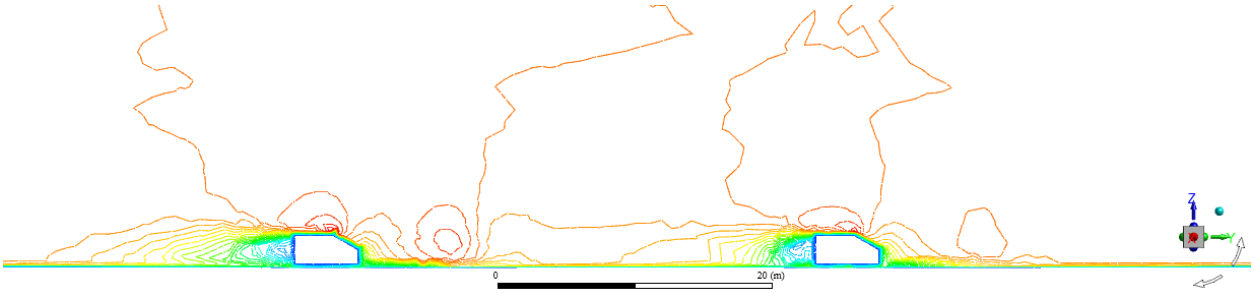

(f)

As illustrated in Figure 24, the distribution of velocity streamlines was mostly around vehicle bodies on each lane although there was recirculation caused by other vehicles on adjacent lanes. For all vehicles, streamlines clustered around their bodies. The cluster appeared to become more noticeable and expanded for trucks than those for sedans and SUVs since trucks did not have any slant angles on their geometry bodies. By comparing two adjacent lanes, one can find the wake effects from vehicles travelling on other lanes. For example, only two small sedans were on the lane in Figure 24 (b), but there was recirculation between two sedans, and note that the flow pattern behind two sedans was different although they were two identical vehicles. It could be explained by that there was a truck on the left lane, Figure 24 (a), behind the following sedan and another truck on the right lane, Figure 24 (c) between two sedans, and the wake flow caused by the trucks resulted in sinuate streamlines in Figure 24 (b). This is why Figure 24 (b) could not have straight velocity streamlines as assumed in the first place even though only two sedans were on that lane. Likewise, the same reason can be applied to explain for the velocity distribution on other lanes.

Additionally, the vertical distribution of CO normalized concentration at three different locations on the highway was compared in Figure 25. When the concentration being normalized, the vehicle height and the volumetric flow rate of emissions were used as weighted average values due to a variety of vehicles traveling on the highway.

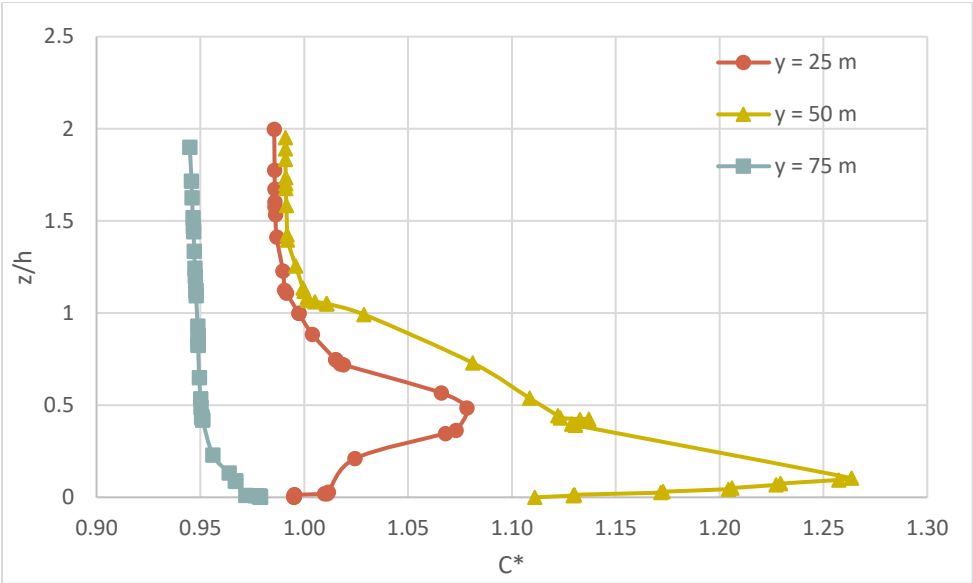

Figure 25. Vertical distribution of normalized concentration at three locations of the highway

The entire length of the highway in the computational domain was 100-meter-long, and all vehicles were moving in the positive y-direction. Therefore, those three locations in Figure 25 corresponded to the downstream of the traffic flow (y = 25 m), the center of the traffic flow (y = 50 m) and the upstream of the traffic flow (y = 75 m). As shown in Figure 25, the center of the traffic flow had the highest normalized emissions concentration, and the upstream of the traffic flow had the lowest normalized emissions concentration. In the computational domain, there was a truck near the center of the highway that contributed to the concentration a lot, so the highest emissions concentration located around the center in the simulated computational domain. For the upstream and the downstream areas, more emissions distributed in the downstream region because the emissions would flow toward the downstream area as time went. Besides, the vehicle wakes influenced the dispersion of the emissions as the concentration peak shown in Figure 25. As mentioned before, the reverse flow and recirculation usually happened in near wakes of vehicles, and the emissions would be likely to be trapped in the recirculation, leaving some emissions behind vehicles that could not dissipate completely and causing relatively high concentration of emissions.

Next, the effects of noise barriers will be investigated. Double T-shaped noise barriers were added in the original computational domain because T-shaped noise barriers had good performance of inhibiting highway emissions from traveling to near highway regions as previous simulation suggested. The velocity streamlines on the central plane of six lanes were displayed in Figure 26.

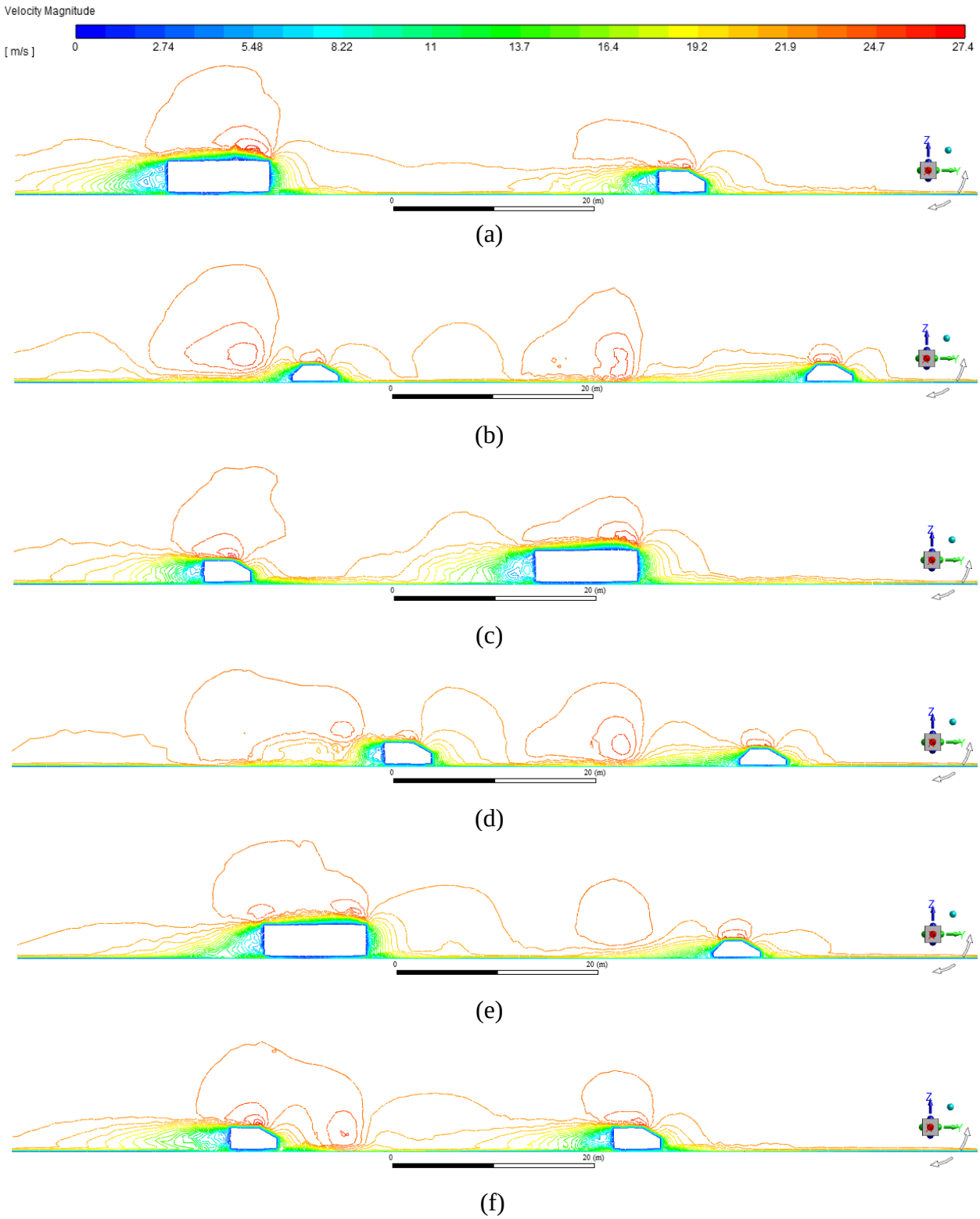

Figure 26. Velocity streamlines with noise barriers on (a) – (f) six lanes

By comparing Figure 26 (cases with noise barriers) with Figure 24 (cases without noise barriers), one can tell that the velocity streamlines did not diverge to very high areas above vehicles. As noise barriers were standing along both sides of the highway, they functioned as boundaries of the highway; hence, the velocity streamlines would not travel haphazardly as described in Figure 24. Other than that, the vehicle wakes were also present, which was independent with the existence of noise barriers. To obtain the effects of noise barriers on the highway emissions, the vertical distribution of CO normalized concentration was compared with the results without noise barriers in Figure 27.

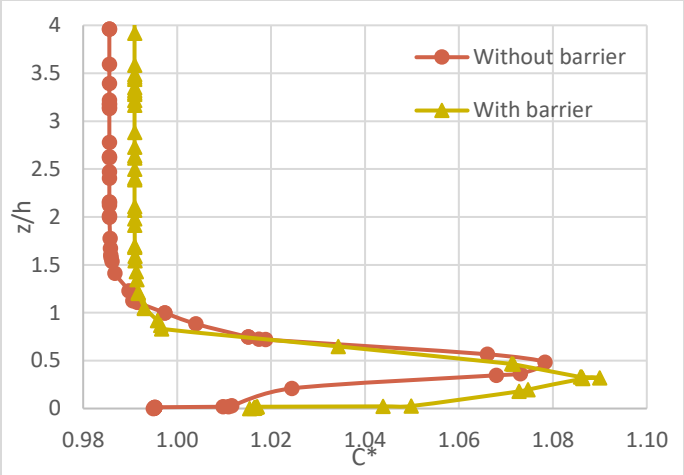

(a) Vertical distribution of normalized concentration at y =25 m

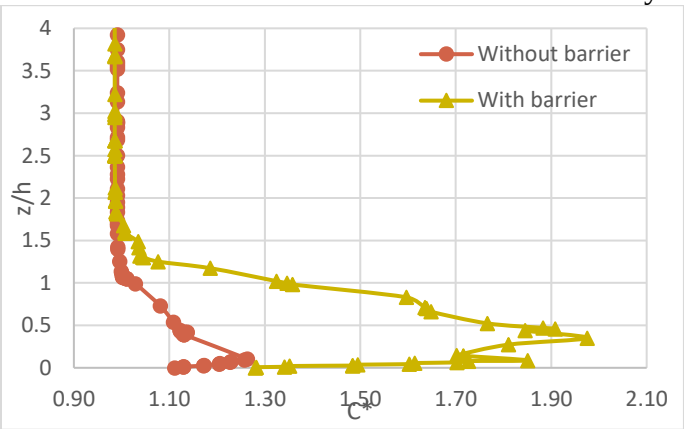

(b) Vertical distribution of normalized concentration at y = 50 m

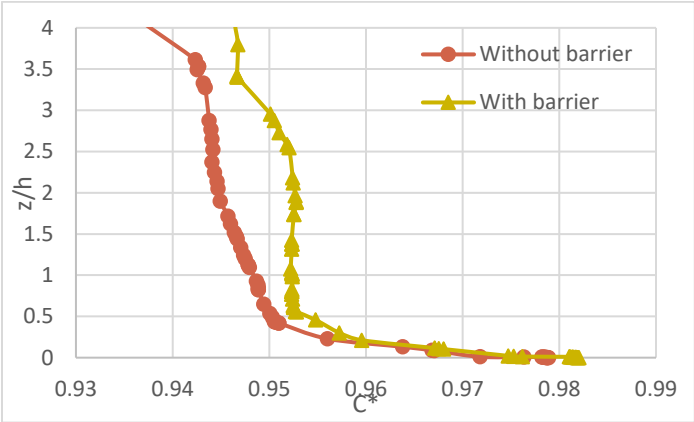

(c) Vertical distribution of normalized concentration at y = 75 m

Figure 27. Comparison of the normalized concentration between with noise barriers and without noise barriers at three locations

Figure 27 suggested that more automobile emissions would remain on the highway if noise barriers were built, especially at the center of the highway, which was consistent with previous simulation results. The center of the highway was already the place where the highest normalized concentration of emissions was found among three locations, and noise barriers made this situation even worse. At the center, the maximum normalized concentration with noise barriers was nearly twice more than that without noise barriers, but the normalized concentration only increased a little for other two locations. It could be concluded that the results of the emissions distribution were possibly related with the velocity results. By comparing Figure 26 (cases with noise barriers) with Figure 24 (cases without noise barriers), when noise barriers were nearby, the velocity streamlines disappeared in a few regions, such as the top of vehicles, which was not conducive to the dispersion of automobile emissions. As a result, the noise barriers behaved as constrains that trapped more automobile emissions on the highway.

3.6 Traffic Flow Effects

This section discussed the effects of traffic flow on the dispersion of automobile emissions on the highway. The traffic flow effects included the effects of vehicle bodies and traffic speed. There are a variety of vehicles in the real life, and different vehicles have different bodies. As the vehicle body would modify the local flow patterns around the vehicle self, the dispersion of emissions was presumed to be influenced by vehicle bodies. On the other hand, the traffic speed would directly affect the velocity magnitude in flow fields, so the dispersion of emissions would also be affected.

3.6.1 Vehicle Body Effects

Three types of vehicles were tested in this paper: sedans, SUVs and trucks. The major difference between vehicle types was their geometry bodies: two slant angles for sedans on both front and rear sides; one slant angle for SUVs on the front side; no slant angle for trucks. In the real life, of course, different vehicles have different emission rates, but the emission rate was considered as the same in this section so as to study the influence caused by vehicle geometry only.

The velocity streamlines for the same type of two vehicles on a single lane are arranged in Figure 28.

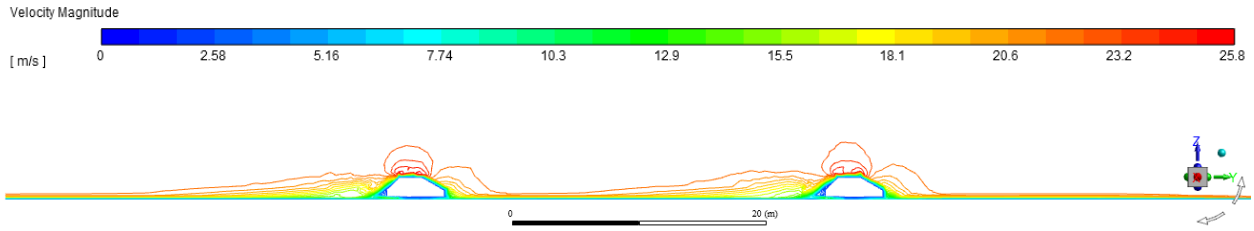

(a) Velocity streamlines for sedans

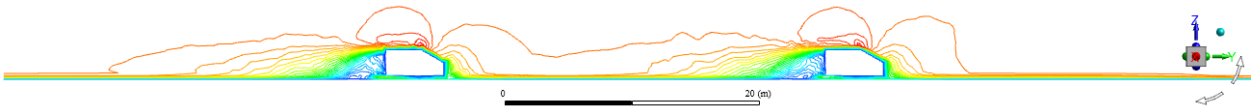

(b) Velocity streamlines for SUVs

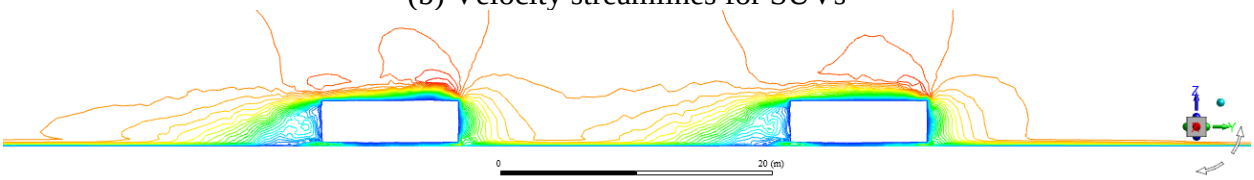

(c) Velocity streamlines for trucks

Figure 28. Comparison of velocity streamlines between three vehicle types

Figure 28 implied that the vehicle geometry clearly modified velocity streamlines. The designed slant angles on vehicles contributed the flow to passing vehicles smoothly and gently. When the upcoming flow attacked vehicles, it had to lift up to pass them. The front slant angle made this process easier for the upcoming flow to climb up, so velocity streamlines bulged greatly in front of trucks. The rear slant angle helped the wake to converge gradually, so velocity streamlines became uniform quickly after passing sedans, whereas there was a long wake left behind SUVs and trucks. Besides, the velocity streamlines above vehicles were also highly impacted. The velocity streamlines bumped a little on the top of sedans but extended higher on the top of trucks. On the other hand, the vehicle height was responsible for the results. Even though sedans and SUVs had the same slant angles on their front sides, the velocity streamlines still became more disturbed in front of SUVs.

In order to show the turbulence affected by vehicle bodies, the contours of turbulent intensity for each type of vehicles are displayed in Figure 29.

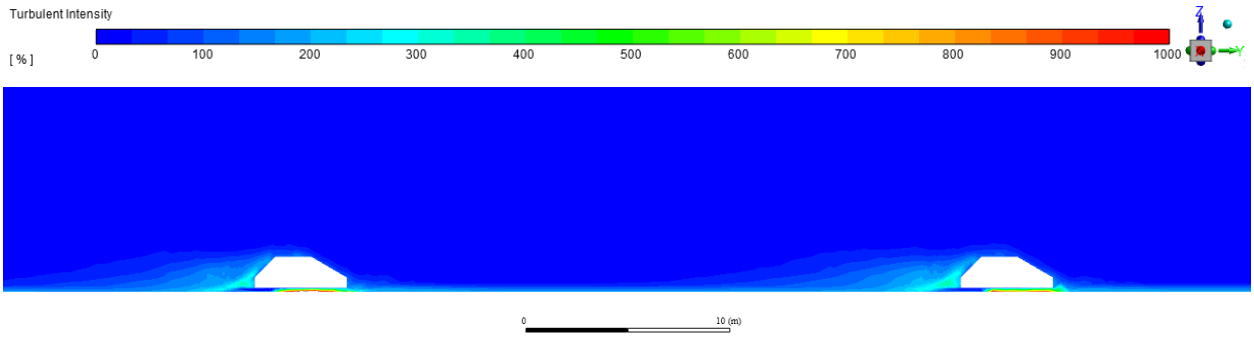

(a) Turbulent intensity for sedans

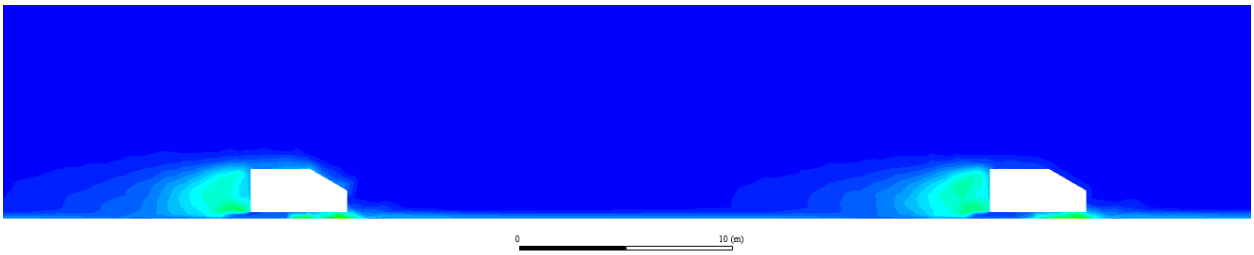

(b) Turbulence intensity for SUVs

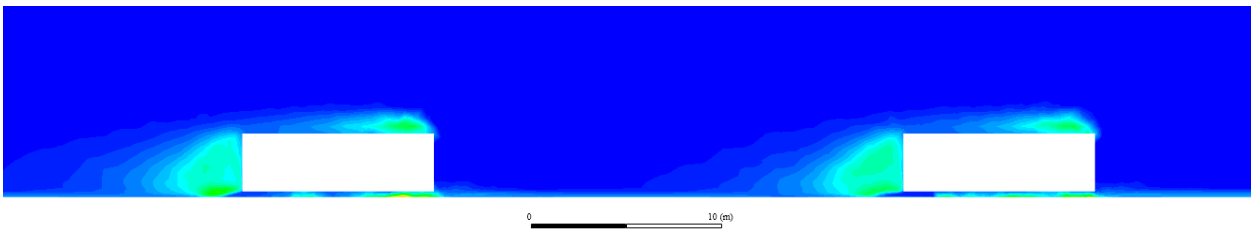

(c) Turbulence intensity for trucks

Figure 29. Comparison of turbulent intensity between three vehicle types

From Figure 29, all vehicles created turbulence behind and under their bodies, but the turbulent intensity was highly influenced by the vehicle geometry. Sedans that had two slant angles created the smallest turbulent areas. SUVs and trucks produced great turbulence behind their bodies that had the same height of vehicles because they did not have rear slant angles. The front slant angle also made a great difference. Sedans and SUVs did not have evident turbulence in their front parts due to the fact that their front slant angles helped the flow pass vehicles smoothly, whereas trucks created large turbulence on the top front edge. In conclusion, turbulence was created around all vehicle bodies, but slant angles helped to decrease the turbulent intensity and areas of turbulence. Front slant angles eliminated the turbulence in the top front area of vehicles, and rear slant angles made the turbulent area behind vehicles small.

To compare the effects of vehicle types on the distribution of CO concentration, the velocity profile and the vertical distribution of the normalized concentration at the center of the highway are shown in Figure 30.

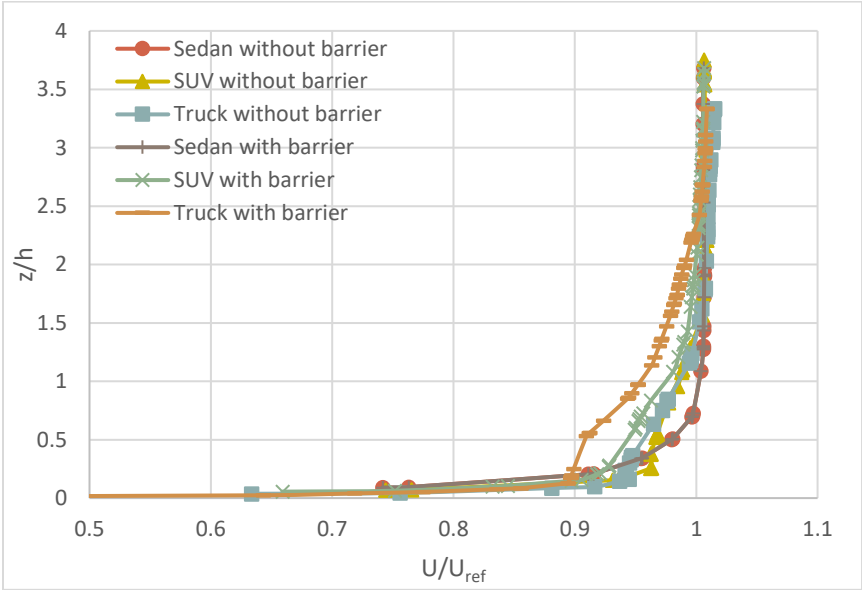

(a) Velocity profiles

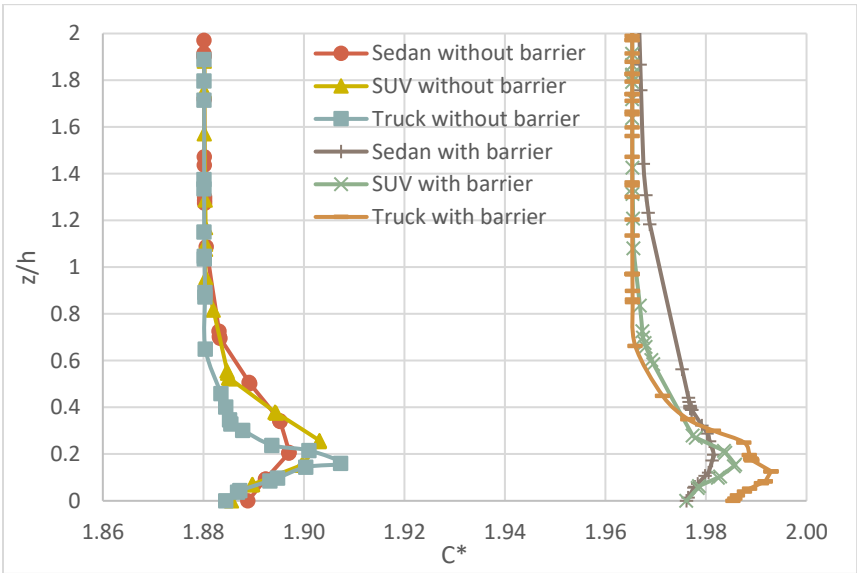

(b) Vertical distribution of normalized concentration

Figure 30. Comparison of velocity profiles and normalized concentration between vehicle types at the center of the highway

Figure 30 (a) suggested all three vehicle types had smaller velocity below twice the height of vehicles when there were noise barriers, which was approximately the height of noise barriers (6 meter). By comparing the velocity between each vehicle type, sedans showed the greatest velocity around the half height of vehicles in both situations with and without noise barriers. The slant angles were also on the top half vehicles, and they modified the flow on the top of vehicles, so Figure 30 (a) had good consistency with the velocity streamlines in Figure 28. Furthermore, the effects of velocity on the emissions distribution could be manifested by large velocity enhancing the transportation of emissions. Accordingly, in Figure 30 (b), the cases with noise barriers resulted in higher normalized concentration of emissions than those without noise barriers, which made agreement again with the noise barrier effects. Trucks presented the highest normalized emissions concentration among three vehicle types because their relatively big bodies without any slant angles made small velocity in the wake flow. Therefore, it can conclude that vehicles with huge bodies and without slant angles trapped much emissions due to small velocity magnitude in their wake flow.

3.6.2 Traffic Speed Effects

This section considered congestion on the highway, which means the traffic flow had low speed. In the simulation, it did not assume that all vehicles had to stop completely in the congestion; instead, lower velocity (40 km/h = 11.11 m/s) was applied to simulate the traffic flow with lower vehicle speed.

Velocity streamlines for low traffic speed on six lanes are displayed in Figure 31.

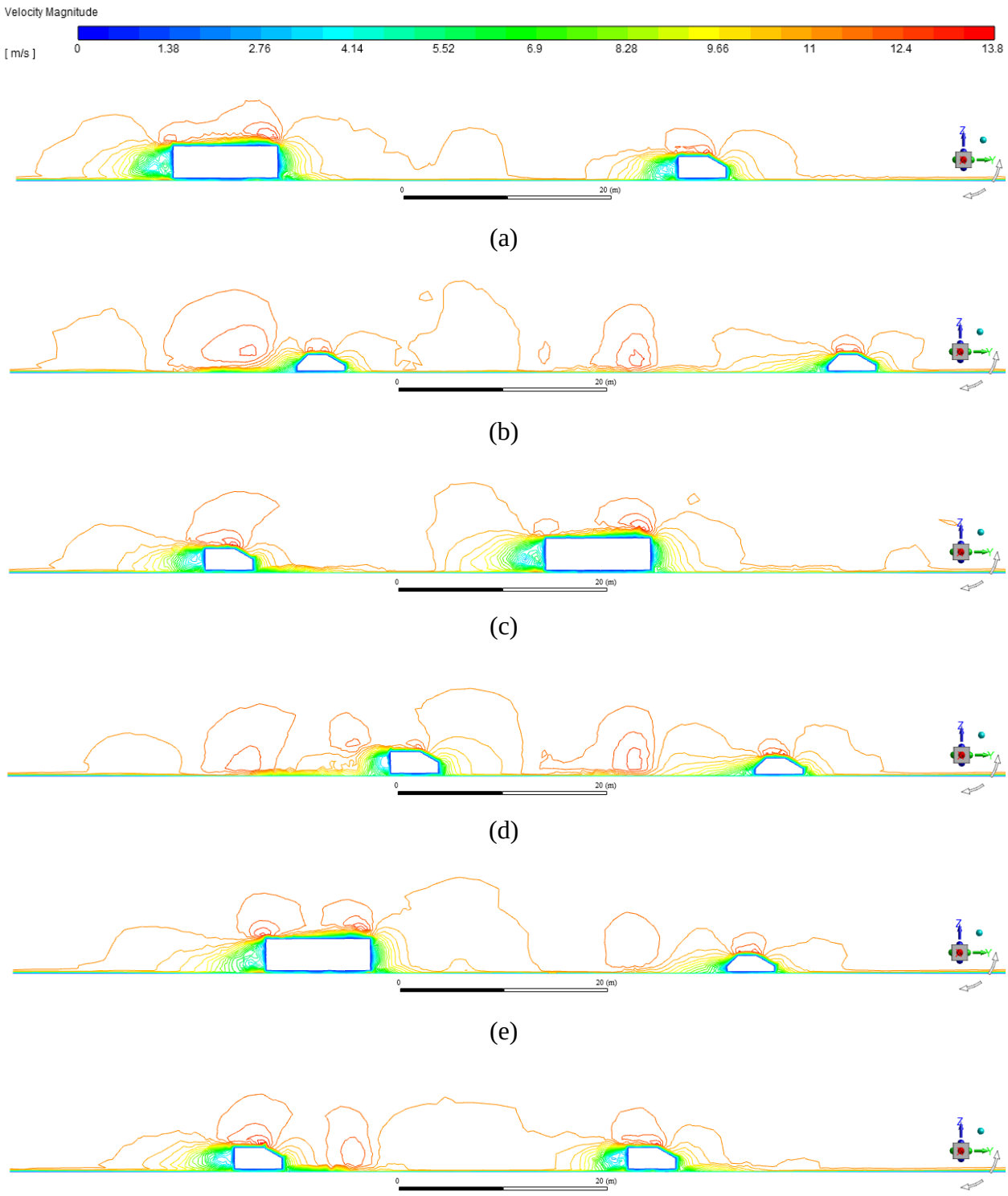

(a)

(b)

(c)

(d)

(e)

(f)

Figure 31. Velocity streamlines for low traffic speed; (a) – (f) six lanes

The velocity magnitude in Figure 26 can be estimated in the colormap. Although the traffic flow had low speed, the wake flow and effects from adjacent lanes could be observed as well. At low traffic speed, all streamlines appeared to surround vehicles instead of continuing to flow further upward as the results of high traffic speed in Figure 24.

Moreover, the effects of traffic speed on automobile emissions on the highway were compared with the results of original traffic speed (80 km/h = 22.22 m/s) in Figure 32.

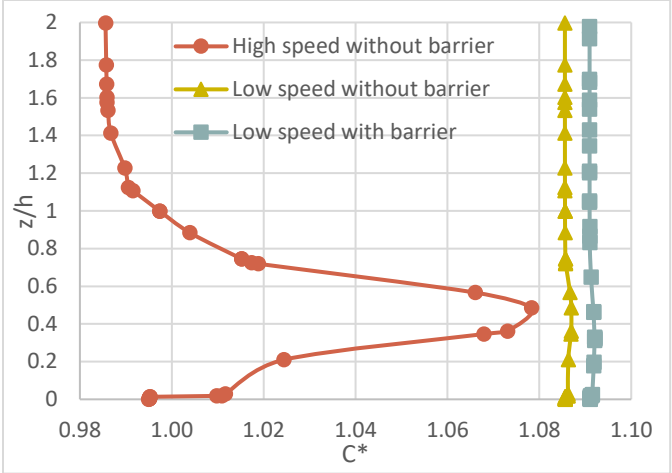

(a) Vertical distribution of normalized concentration at y = 25 m

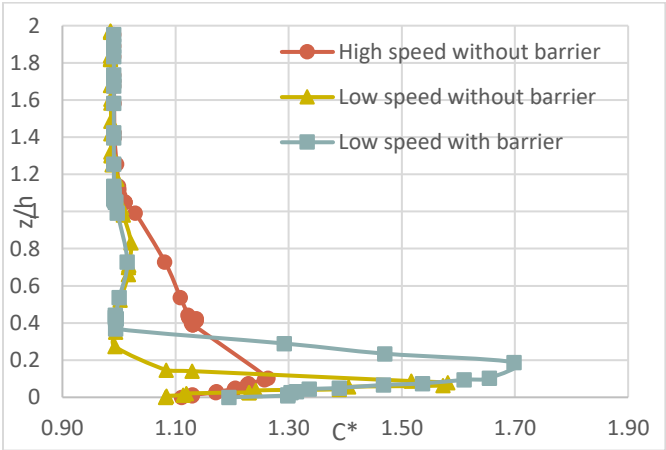

(b) Vertical distribution of normalized concentration at y = 50 m

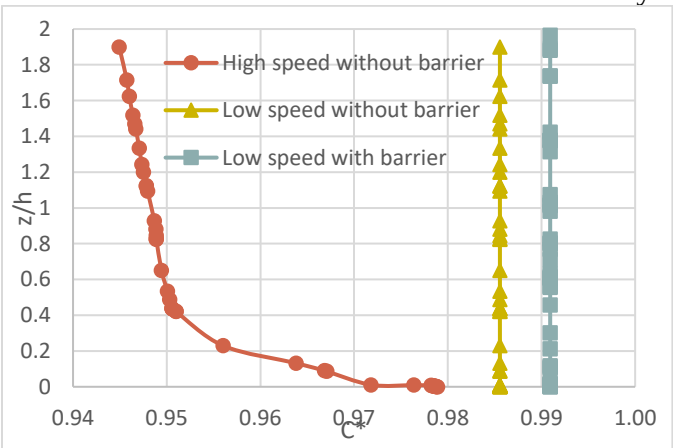

(c) Vertical distribution of normalized concentration at y = 75 m

Figure 32. Comparison of normalized concentration between different traffic speed

As shown in Figure 32, when the traffic flow was at a low speed, the CO normalized concentration on the highway would increase. In other words, when traffic congestion happened on highways, it would not be helpful for the transportation and dispersion of automobile emissions. The major cause was probably that the advection effect was weak as the flow velocity decreased in congested conditions. Most of emissions were collected near the ground and in downstream areas, which agreed with the previous research [24]. In Figure 32 (a) and (c), the distribution of normalized emissions concentration for low traffic speed was nearly stagnant compared with the results for high traffic speed. Nevertheless, in Figure 32 (b), i.e. the center of the highway, the distribution became complicated. The peak normalized concentration occurred near the ground when the traffic speed was low. There was much heavier traffic around the center of the highway than the upstream and downstream areas, so the distribution of emissions would not be simply affected by the traffic speed as suggested in Figure 32 (a) and (c). Note that there was a truck near the center of the highway, so its shape also contributed to the results in Figure 32 (b), making that noticeably large normalized concentration.

As a result, when the traffic flow on the highway had low speed, automobile emissions would rather sink and gather onto the ground. Again, the noise barriers always increased the concentration of emissions no matter how fast or slow vehicles travelled on the highway.

4. CONCLUSIONS AND FUTURE WORK

Numerical models have been developed to study the dispersion of automobile emissions near and on the highway due to the effects of noise barriers and different traffic flow conditions. This thesis was divided into multiple sections to study the different factors that exert effects on highway automobile emissions. First, the numerical simulation was validated by wind tunnel experiments from the literature. Good agreement was found in the simulation results when comparing with experimental data. Then simulation and analysis were conducted under various highway configurations and traffic flow conditions.

Noise barrier shape effects were first introduced by comparing simulation results between rectangular and T-shaped noise barriers. The contours of CO dispersion and the vertical distribution of normalized concentration on the highway, near the highway and in the far downstream area were investigated. The results showed that noise barriers impeded the dispersion of automobile emissions in downstream areas while trapped great amount of emissions on the highway. The results also suggested that T-shaped noise barriers could help to improve the air quality in downstream areas, which had better effects than rectangular noise barrier. Nevertheless, the level of emission reduction was dependent on the top length and height of T-shaped noise barriers. In other words, the ratio of the top length to height was a critical parameter for T-shaped noise barriers. The shape effects of highway noise barrier on the dispersion of automobile emissions were not significant at the location of the highway and far downstream regions because much emissions were always trapped on the highway and the emissions had already become very little in far downstream areas. However, the emission dispersion varied with noise barrier shapes in near-highway regions; for example, in the 10 times noise barrier height far downstream region, T-shaped noise barriers could have better performance on reducing the emission concentration downstream than rectangular ones. Consequently, communities and residential areas would better be at least 10 times noise barrier height far away from highways. For T-shaped noise barriers, it suggested that the ratio of the top length to the height determined their performances on reducing automobile emissions near highways. The optimized ratio was around 0.2, which would be used in later simulation and design of T-shaped noise barriers.

In addition to noise barrier shape effects, the influence of inflow conditions was studied next based on those two noise barrier shapes. The simulation results implied that noise barrier shape effects were highly dependent on the inflow conditions. After the wind passing noise barriers, there could be swirls behind noise barriers due to the existence of noise barriers on the way the wind going through. The swirls would be corresponded to the shapes of noise barrier so that the emissions dispersion downstream would be influenced. Different inflow conditions create different wind shear and turbulence. The uniform inflow doesn't have wind shear, but the linear inflow and the power law inflow do. As a result, the best case under the power law would not necessary be the best one under linear or uniform inflow conditions. The combination of wind speed, wind shear and turbulence intensity influenced the dispersion of automobile emissions. When the inflow condition could create large velocity and wind shear, it was supposed to improve the dispersion of automobile emissions.

Thirdly, moderate traffic flow was added on the highway to make the simulation much closer to the real life. The traffic flow was modeled on a one-way six-lane highway with and without double T-shaped noise barriers beside the highway. Three different types of vehicle models were generated to represent sedans, SUVs and trucks. Numerical simulation results illustrated velocity streamlines on the central plane of each lane and vertical distribution of CO normalized emissions concentration at the upstream, the center and the downstream of the highway. The automobile wakes were able to be observed in velocity streamlines and independent with the existence of noise barriers; however, the emissions concentration appeared to become more on the highway when T-shaped noise barriers were present. As a result, the noise barriers acted as boundaries for the flow across the highway and thus trapped more automobile emissions on the highway. Intuitively, the concentration of emissions would decrease with height, but from the vertical distribution of concentration, concentration inversion could happen due to the automobile wakes. The distribution results suggested that the center of the highway had the highest emissions concentration and the downstream area of the traffic flow had the second highest concentration.

At last, the effects from vehicle geometry bodies and traffic speed were also investigated. When slant angles were designed for both front and rear sides of vehicles, the velocity streamlines would not fluctuate too much while passing these vehicles. Therefore, the automobile emissions could be

pushed to transport and disperse. As for those vehicles without any slant angles, they worked as barriers that impeded the flow and hence the dispersion of emissions even though they were moving, so they trapped more emissions than other types of vehicles. As a result, large vehicles, such as trucks, should be limited in densely populated areas. When the traffic flow had low speed, for instance when congestion happened, the emissions concentration would remain more on the highway because such small velocity magnitude could not really contribute to the dispersion of automobile emissions. Consequently, there should be a minimum speed limit on highways, and traffic jams should be avoided as much as possible.

Overall, this research conducted a comprehensive modeling and simulation to study multiple factors that influence the dispersion of highway automobile emissions. Detailed analysis results for the dispersion of automobile emissions were presented: effects from noise barriers, different inflow conditions and various traffic flow conditions. More representative automobile emissions, such as nitrogen oxides and particle matters, and possible reactions between them, such as water evaporation and other chemical reactions, should be taken into consideration for future work. Local meteorology can also be considered, such as temperature and humidity at daytime and night.

REFERENCES

[1] M. Brauer; G. Hoek; P. Van Vliet; K. Meliefste; P.H. Fischer; A. Wijga; L.P. Koopman; H.J. Neijens; J. Gerritsen; M. Kerkhof. Air pollution from traffic and the development of respiratory infections and asthmatic and allergic symptoms in children. *Am. J. Respir. Crit. Care.* 2002, Vol. 166, pp. 1092–1098.

[2] J. Currie; R. Walker. Traffic congestion and infant health: evidence from E-ZPass. *AEJ Appl. Econ.* 2011, Vol. 3, pp. 65–90.

[3] L. Schweitzer; J.P. Zhou. Neighborhood Air Quality, Respiratory Health, and Vulnerable Populations in Compact and Sprawled Regions. *JAPA.* 2010, Vol. 76, pp. 363–371.

[4] The 2018 EPA Automotive Trends Report. Retrieved from https://www.epa.gov/automotive-trends/download-automotive-trends-report#Full%20Report.

[5] Best Practices for Reducing Near-Road Pollution Exposure at Schools. Retrieved from https://www.epa.gov/sites/production/files/201510/documents/ochp_2015_near_road_pollution_booklet_v16_508.pdf.

[6] D.K. Heist.; S.G. Perry.; L.A. Brixey. A wind tunnel study of the effect of roadway configurations on the dispersion of traffic-related pollution. *Atmos. Environ*. 2009, Vol. 43, pp. 5101–5111.

[7] S. Amini; F.E. Ahangar; N. Schulte; A. Venkatram, Using models to interpret the impact of roadside barriers on near-road air quality. *Atmos. Environ.* 2016, Vol. 138, pp. 55–64.

[8] L.Y. Gong; X.L. Wang. Numerical study of noise barriers' side edge effects on pollutant dispersion near roadside under various thermal stability conditions. *Fluids.* 2018, Vol. 3, pp. 105–122.

[9] W.E. Scholes; A.C. Salvidge; J.W. Sargent. Field performance of a noise barrier. *J. Sound Vib.* 1971, Vol. 16, pp. 627–642.

[10] T. Ishizuka; K. Fujiwara. Performance of noise barriers with various edge shapes and acoustical conditions. *Appl. Acoust.* 2004, Vol. 65, pp. 125–141.

[11] M. Baulac; J. Defrance; P. Jean. Optimization with genetic algorithm of the acoustic performance of T-shaped noise barriers with a reactive top surface. *Appl. Acoust.* 2008, Vol. 69, pp. 332–342.

[12] W. Shao; H.P. Lee; S.P. Lim. Performance of noise barriers with random edge profiles. *Appl. Acoust.* 2001, Vol. 62, pp. 1157–1170.

[13] T. Van Renterghem; D. Botteldooren. Numerical simulation of the effect of trees on downwind noise barrier performance. *Acta Acust.* 2003, Vol. 89, pp. 764–778.

[14] G.S.W. Hagler; W. Tang; M.J. Freeman; D.K. Heist; S.G. Perry; A.F. Vette. Model evaluation of roadside barrier impact on near-road air pollution. *Atmos. Environ.* 2011, Vol. 45, pp. 2522–2530.

[15] D. Finn; K.L. Clawson; R.G. Carter; J.D. Rich; R.M. Eckman; S.G. Perry; V. Isakov; D.K. Heist. Tracer studies to characterize the effects of roadside noise barriers on near-road pollutant dispersion under varying atmospheric stability conditions. *Atmos. Environ.* 2010, Vol. 44, pp. 204–214.

[16] J.T. Steffens; D.K. Heist; S.G. Perry; K.M. Zhang. Modeling the effects of a solid barrier on pollutant dispersion under various atmospheric stability conditions. *Atmos. Environ.* 2013, Vol. 69, pp. 76–85.

[17] N. Zhou; J. Chen; D.E. Adams; S. Fleeter. Influence of inflow conditions on turbine loading and wake structures predicted by large eddy simulations using exact geometry. *Wind Energy.* 2016, Vol. 19, pp. 803–824.

[18] N.S. Uzol; O. Uzol. Effect of steady and transient wind shear on the wake structure and performance of a horizontal axis wind turbine rotor. *Wind Energy.* 2013, Vol. 16, pp. 1–17.

[19] K.S. Rao; R.L. Gunter; J.R. White; R.P. Hosker. Turbulence and dispersion modeling near highways. *Atmos Environ.* 2002, Vol. 36, pp. 4337–4346.

[20] A. Alonso-Estebanez; P. Pascual-Munoz; C. Yague; R. Laina; D. Castro-Fresno. Field experimental study of traffic-induced turbulence on highways. *Atmos Environ.* 2012, Vol. 61, pp. 189–196.

[21] U. Bhautmage; S. Gokhale. Effects of moving-vehicle wakes on pollutant dispersion inside a highway road tunnel. *Environmental Pollution*. 2016, Vol. 218, pp. 783–793.

[22] M. Carpentieri; P. Kumar; A. Robins. Wind tunnel measurements for dispersion modelling of vehicle wakes. *Atmos Environ.* 2012, Vol. 62, pp. 9–25.

[23] M. Karim; H. Matsui. A mathematical model of wind flow, vehicle wake, and pollutant concentration in urban road microenvironments. Part I: model description. *Transportation Research Part D: Transport and Environment*. 1998, Vol. 3, pp. 81–92.

[24] J.L. Dong; Y. Tao; Y.M. Xiao; J.Y. Tu. Numerical simulation of pollutant dispersion in urban roadway tunnels. *The Journal of Computational Multiphase Flows*. 2017, Vol. 9, pp. 26–31.

[25] J.F. Huang; T.L. Chan. Vehicle queue effect on the characteristics of air flow, and exhaust scalar dispersion and distribution fields in the vehicle wake. *International Journal of Heat and Mass Transfer*. 2012, Vol. 55, pp. 7981–7990.

[26] Y. Kim; L. Huang; S.L. Gong; C.Q. Jia. A new approach to quantifying vehicle induced turbulence for complex traffic scenarios. *Chinese Journal of Chemical Engineering*. 2016, Vol. 24, pp. 71–78.

[27] Anderson J.D. Computational Fluid Dynamics: The Basics with Applications, 1st ed.; McGraw-Hill, Inc.: NY, USA, 1995.

[28] Fluent Theory Guide: Standard, RNG, and Realizable k-ε Models. Retrieved from https://ansyshelp.ansys.com/account/secured?returnurl=/Views/Secured/corp/v191/flu_th/flu_th_sec_turb_all_ke.html.

[29] Fluent Theory Guide: Standard, BSL, and SST k-ω Models. Retrieved from https://ansyshelp.ansys.com/account/secured?returnurl=/Views/Secured/corp/v191/flu_th/flu_th_sec_turb_komega.html.

[30] Fluent Theory Guide: Realizable k-ε model. Retrieved from https://ansyshelp.ansys.com/account/secured?returnurl=/Views/Secured/corp/v191/flu_th/flu_th_sec_turb_realizke.html.

[31] Fluent Theory Guide: Species transport equations. Retrieved from https://ansyshelp.ansys.com/account/secured?returnurl=/Views/Secured/corp/v191/flu_th/flu_th_sec_species_trans_eq.html.

[32] Indiana Driver's Manual, Chapter 5: Safe Vehicle Operation. Indiana Bureau of Motor Vehicles, 2018, pp. 69.